Modeling the reactive halogen plume from Ambrym and its impact on the troposphere with the CCATT-BRAMS mesoscale model

L. Jourdain[1], T.J. Roberts[1], M. Pirre[1], B. Josse[2]

[1]{ Laboratoire de Physique et de Chimie de l'Environnement et de l'Espace (LPC2E), Université d'Orléans, CNRS, Orléans, France}

[2]{ CNRM-GAME, Météo-France and CNRS, Toulouse, France}

Correspondence to: L. Jourdain (line.jourdain@cnrs-orleans.fr)

Abstract:

Ambrym volcano (Vanuatu, Southwest Pacific) is one of the largest sources of continuous volcanic emissions worldwide. As well as releasing SO_2 that is oxidized to sulfate, volcanic plumes in the troposphere are shown to undergo reactive halogen chemistry whose atmospheric impacts have been little explored to date. Here, we investigate with the regional scale model CCATT-BRAMS the chemical processing in the Ambrym plume and the impact of this volcano on the atmospheric chemistry at both local and regional scales. We focus on an episode of extreme passive degassing that occurred in early 2005 and for which airborne DOAS measurements of SO_2 and BrO columns, in the near downwind plume between 15 and 40 km from the vents, have been reported. The model was developed to include reactive halogen chemistry and a volcanic emission source specific to this extreme degassing event. In order to test our understanding of the volcanic plume chemistry, we performed very high resolution (500 m x 500 m) simulations using the model nesting grid capability and compared "point-by-point" each DOAS measurement to its temporally and spatially interpolated model counterpart. Simulated SO_2 columns show very good quantitative agreement with the DOAS observations, suggesting that the plume direction as well as its dilution in the near downwind plume are well captured. The model also reproduces the salient features of volcanic chemistry

as reported in previous work such as HO_x and ozone depletion in the core of the plume. When a high-temperature chemistry initialization is included, the model is able to capture the observed BrO/SO_2 trend with distance from the vent. The main discrepancy between observations and model is the bias between the magnitudes of observed and simulated BrO columns that ranges from 60 % (relative to the observations) for the transect at 15 km to 14 % for the one at 40 km from the vents. We identify total in-plume depletion of ozone as a limiting factor to the partitioning of reactive bromine into BrO in the near source (concentrated) plume under these conditions of extreme emissions and low background ozone concentrations (15 ppbv). Impacts of Ambrym in the Southwest Pacific region were also analyzed. As the plume disperses regionally, reactive halogen chemistry continues on sulfate aerosols produced by SO_2 oxidation and promotes BrCl formation. Ozone depletion is weaker than at the local scale but still between 10 to 40% , in an extensive region a few thousands of kilometres from Ambrym. The model also predicts transport of bromine to the upper troposphere and stratosphere associated with convection events. In the upper troposphere, HBr is re-formed from Br and HO_2. Comparison of SO_2 regional scale model fields with OMI satellite SO_2 fields confirms that the Ambrym SO_2 emissions estimate based on the DOAS observations used here is realistic.

The model confirms the potential for volcanic emissions to influence the oxidizing power of the atmosphere: methane lifetime (calculated with respect to OH and Cl) is overall increased in the model due to the volcanic emissions. When considering reactive halogen chemistry, that depletes HOx and ozone, the lengthening of methane lifetime with respect to OH is increased by a factor of 2.6 compared to a simulation including only volcanic SO_2 emissions. Cl radicals produced in the plume counteract 41% of the methane lifetime lengthening due to OH depletion. Including the reactive halogen chemistry in our simulation also increases the

50 lifetime of SO_2 in the plume with respect to oxidation by OH by 36% compared to a
51 simulation including only volcanic SO_2 emissions. This study confirms the strong influence of
52 Ambrym emissions during the extreme degassing event of early 2005 on the composition of
53 the atmosphere at both local and regional scales. It also stresses the importance of considering
54 reactive halogen chemistry when assessing the impact of volcanic emissions on climate.
55

56 ## 1. Introduction

57 Volcanic activity is a source of climatically and environmentally important gases and aerosols
58 in the atmosphere. To this respect, much work has focused on the climate impact of sulfur
59 compounds injected by major volcanic explosions into the stratosphere. In this layer, they are
60 converted into sulfate aerosols that have a long residence time (~1-2 years) and can affect
61 climate directly via the perturbation of the Earth‘s radiation balance as well as indirectly due
62 to the strong coupling between radiation, microphysics and atmospheric chemistry in the
63 stratosphere. This forcing from volcanic stratospheric aerosols is now well understood and is
64 thought to be the most important natural cause of externally forced climate change on the
65 annual but also on the multi-decadal time scales and hence is thought to explain the majority
66 of the pre-industrial climate change of the last millennium (Myrhe at al., 2013).
67 On the other hand, the impact of other compounds as halides (HCl, HBr) injected by
68 explosive eruptions into the stratosphere as well as the overall impact of minor eruptions and
69 quiescent passive degassing have been largely overlooked. However, the presence of volcanic
70 halogens in the stratosphere following explosive eruptions has been recently detected (e.g.,
71 Hunton et al., 2005; Rose et al., 2006; Prata et al., 2007; Theys et al., 2014, Carn et al.,
72 2016). Such volcanic halogen injection, enabled by incomplete volcanic halides washout as
73 first predicted by a model study (Textor et al., 2003), was found to cause enhanced reactive
74 chlorine and bromine as well as enhanced ozone depletion (Rose et al., 2006; Millard et al.,

2006). As a result, it is important, as emphasized in Cadoux et al. (2015), to consider volcanic halogens in addition to sulfur compounds when studying the influence on the stratosphere of past and future explosive eruptions.

Until recently, the impact of quiescent degassing and of minor eruptions have also been largely overlooked because of the lower lifetime of volcanic emissions in the troposphere. However, it was shown that quiescent degassing alone is responsible for a high proportion (~30–70 %) of the volcanic SO_2 flux to the atmosphere (Andres and Kasgnoc, 1998; Halmer et al., 2002; Mather et al., 2003). In addition, quiescent degassing as well as minor eruptions were found to contribute more to the sulfur load in the free troposphere in regard to their emissions compared to stronger oceanic and anthropogenic sources due to the elevation of most volcanoes (e.g., Chin and Jacob, 1996; Graf et al., 1997). Furthermore, recent studies show the need for a better knowledge of the tropospheric concentrations of natural aerosols and their precursor gases to quantify the aerosol indirect forcing from anthropogenic activities due to nonlinearities in the relations linking aerosol concentrations and cloud albedo (Carslaw et al., 2013; Schmidt et al., 2012). Volcanic emissions in the troposphere have also been recognized to cause environmental and health problems due to the deposition of SO_2, sulfate, hydrogen halides (mainly HCl and HF) and toxic metals (for a review, see Delmelle, 2003) as well as adversely impacting air quality.

Finally, there is also evidence of chemical reactivity in tropospheric plumes with consequences on the oxidizing power of the troposphere (and hence effects on climate) as well as on the deposition of mercury (e.g., von Glasow, 2010). Indeed, reactive halogens as BrO (e.g., Bobrowki et al., 2003; Lee et al., 2005; Oppenheimer et al., 2006; Bobrowski and Platt, 2007; Bani et al., 2009; Kern et al., 2009; Theys et al., 2009; Boichu et al., 2011; Kelly et al., 2013; Hörmann et al., 2013; Bobrowski et al., 2015) as well as OClO (Bobrowski et al., 2007; General et al., 2014, Gliß et al., 2015) have been detected in the plumes of many

100 volcanoes worldwide. Observations of ClO have also been reported (Lee et al., 2005) but are
101 subject to some uncertainties (see Roberts et al., 2009). For BrO, it is clear that its formation
102 results from the conversion of the emitted volcanic HBr gas into reactive bromine in the
103 presence of sulfate aerosols (Oppenheimer et al., 2006, Bobrowski et al., 2007, Roberts et al.,
104 2009, Von Glasow, 2010). Central to this chemical mechanism, first identified in the context
105 of arctic spring ozone depletion events (Fan and Jacob, 1992), is the reactive uptake of HOBr
106 on the sulfate aerosol. The net result is release of gaseous reactive bromine from the sulfate
107 aerosol (initially as Br_2, which then converts into other forms including Br, BrO, HOBr,
108 $BrONO_2$) and depletion of oxidants O_3, HO_2 as well as NO_2. Reactive bromine acts as a
109 catalyst to its own formation, leading to an exponential growth called "bromine explosion"
110 also observed in the arctic during spring (e.g., Barrie et al., 1988), in the marine boundary
111 layer (e.g., Saiz Lopez et al., 2004) and over salt lakes (e.g., Hebestreit et al., 1999) (for a
112 review see Simpson et al., 2015). Following the first discovery of volcanic BrO (Bobrowski et
113 al., 2003), depletion of ozone has also been observed in volcanic plumes (Vance et al. 2010;
114 Oppenheimer et al. 2010; Schuman et al., 2011; Kelly et al., 2013; Surl et al. 2015). The
115 plume atmospheric chemistry is also highly influenced by the degree of plume mixing with
116 entrained ambient air (Roberts et al., 2014a).
117 Owing to the numerous environmental and climate impacts of quiescent degassing and minor
118 eruptions occurring in the troposphere, it is important to take these volcanic sources into
119 account in the 3D atmospheric models (regional and global models) that aim to understand the
120 chemical composition of the atmosphere, its evolution and its interaction with climate. This
121 paper is an attempt to do that and builds on previous modeling work. The numerical 1D
122 models MISTRA and PlumeChem (e.g., Bobrowski et al., 2007; Roberts et al., 2009, 2014a;
123 von Glasow et al., 2010; Boichu et al. 2011; Kelly et al., 2013) are able to broadly reproduce
124 observed ratios of BrO to SO_2 with distance downwind from volcanoes as well as simulate

125 ozone depletion (e.g., Roberts et al., 2014a; Surl et al., 2015). These modeling studies show
126 the need to take into account the high temperature chemistry following the mixing of volcanic
127 gas with ambient air in order to reproduce the timing of BrO formation. Indeed, high-
128 temperature model studies (Gerlach, 2004; Martin et al., 2006; Martin et al., 2009) have
129 predicted that the mixing of volcanic gases and air at the vent leads to high temperature
130 oxidative dissociation and hence to the formation of radical species. These species accelerate
131 the onset of this chemistry, the formation of BrO being autocatalytical and driven forwards by
132 low-temperature reactions occurring on volcanic aerosol. To date, simulations of reactive
133 halogen (BrO_x, ClO_x) chemistry in volcanic plumes and its impacts have been restricted to 1D
134 and box model studies.
135 Here, we present a 3D regional model study of the impact of Ambrym volcano emissions, not
136 only of sulfur emissions but also of halogen emissions including their reactive chemistry, on
137 the chemical composition of the troposphere at both local and regional scales. Ambrym
138 volcano, Vanuatu, is recognized as a significant contributor to the global volcanic flux of SO_2
139 (Bani et al., 2012; Allard et al., 2009, 2015) as well as of halogen halides HF, HCl, HBr
140 (Allard et al. 2009, 2015). Our focus is an extreme degassing episode that occurred in early
141 2005, for which airborne DOAS SO_2 and BrO columns in the plume (15- 40 km of the vents)
142 have been reported (Bani et al., 2009).
143 The paper is organised as follows. In section 2, we briefly present the Ambrym volcano and
144 the main chemical reactions of volcanic plumes. We also present the reported measurements
145 and detail the model developments made in this study. In section 3, we first test our
146 understanding of the plume chemistry at the plume level by comparing "point by point" the
147 model fields with the DOAS SO_2 and BrO columns in the near downwind plume as well as
148 performing some sensitivity studies. The local impact of Ambrym plume is also presented. In

149 section 4, the regional impact of Ambrym plume is analyzed and discussed. The conclusions
150 are presented in section 5.
151
152 **2. Methods**
153 **2.1 The Context: Ambrym volcano and volcanic plume chemistry**
154 **2.1.1 Ambrym volcano**
155 The Vanuatu Arc is a group of about 80 islands and islets located in the Southwest Pacific
156 that was formed and had continued to evolve as a result of the complex interaction between
157 the Pacific plate and the Indo-Australian plate (Robin et al., 1993). Ambrym (160°08'E,
158 16°15'S) situated in the central zone of the Vanuatu arc is a basaltic stratovolcano of 50 km
159 long and 35 km wide rising 1334 meters above sea level. It has in its center a 12 km diameter
160 caldera with two active cones Mounts Marum and Benbow filled with permanent lava lakes.
161 It has recently been highlighted that the Vanuatu arc is one of the most important entry points
162 for volcanic gases into the atmosphere with mean annual emission of 3Tg/yr of SO_2 estimated
163 for the period 2004-2009 representing about 20 % of the global volcanic SO_2 annual
164 emissions (Bani et al., 2012). Under normal quiescent degassing conditions, Ambrym volcano
165 has a mean emission of 5.44 kt/day of SO_2, comparable with Mt Etna (Italy), and hence
166 contributes to two-thirds of the total budget of the arc (Bani et al., 2012). It is also a
167 significant contributor to the global volcanic flux for several other species (Allard et al., 2009;
168 2015). The volcano impact on the population and environment includes crop damage and food
169 shortages due to deposition of halogen acids, SO_2 and H_2SO_4 as well as dental fluorosis due to
170 the water contamination by wet deposition of fluorine (Allibone et al., 2010). The volcano
171 impact on sulfate aerosol in the Southwest Pacific has also recently been investigated
172 (Lefèvre et al., 2015). They found a strong signal in the aerosol optical depth (AOD) from
173 MODIS (Moderate Resolution Imaging Spectroradiometer) due to Ambrym sulfur emissions;

this signal contributes 15 % to the total AOD as far as 1500 km from the volcano. Here, we focus on the halogen impact alongside sulfur. We study an event of extreme passive degassing that took place in January 2005 when the SO_2 emission was more than 3 times higher than its mean value over the 2004-2009 period (Bani et al. 2012). This extreme degassing occurred as a pulse of several months duration (Bani et al., 2012). Our study evaluates impacts from the continuous degassing on 12th January, enabling comparison to plume BrO and SO_2 measurements from a field campaign (Bani et al., 2009).

2.1.2 Volcanic plume chemistry

Reactions R1-R7 illustrate the autocatalytic conversion of volcanic HBr into reactive bromine species and the associated catalytic ozone depletion (for a more complete set of reactions, see Simpson et al., 2007). A key reaction is the heterogeneous reaction of HOBr with Br^- (from dissolved volcanic HBr) and H^+ in volcanic sulfate aerosols (R1) that results in the production of Br_2. Once released to the gas-phase, Br_2 is rapidly photolysed to give 2 Br radicals (R2), which can react with ozone to form BrO (R3). The reaction of BrO with HO_2 (R5) reform HOBr that can again react on the sulfate aerosol (R1) to further propagate the cycle, each time doubling the concentration of reactive bromine. In addition to reactive uptake of HOBr, hydrolysis of $BrONO_2$ (R7) into sulfate aerosol can also regenerate HOBr that can undergo another cycle.

R1 $$HOBr_{(aq)} + Br^-_{(aq)} + H^+_{(aq)} \rightarrow Br_{2(aq->g)} + H_2O_{(l)}$$

R2 $$Br_2 \xrightarrow{h\nu} 2Br$$

R3 $$Br + O_3 \rightarrow BrO + O_2$$

R4a $$BrO + BrO \rightarrow 2Br + O_2$$

R4b $$BrO + BrO \rightarrow Br2 + O_2$$

197 R5 $BrO + HO_2 \rightarrow HOBr + O_2$

198 R6 $BrO + NO_2 \rightarrow BrONO_2$

199 R7 $BrONO_2 + H_2O(l) -> HOBr + HNO_3$

200 Because BrO can be photolyzed and the resulting O quickly reacts with O_2 to give back O_3,
201 the key ozone destruction steps are reactions R3 together with reactions R4a, R4b, R5 and R6
202 (von Glasow et al., 2009). Note, that BrCl can be the product of the reactive uptake of HOBr
203 (R8) when Br^- becomes depleted, leading to non-autocatalytic formation of reactive chlorine.

204 R8 $HOBr_{(aq)} + H^+_{(aq)} + Cl^-_{(aq)} \rightarrow BrCl_{(aq \rightarrow g)} + H_2O_{(l)}$

205

206 **2.2 Measurements**

207 **2.2.1 DOAS Data**

208 We use DOAS (Differential Optical Absorption Spectroscopy) measurement of SO_2 and BrO
209 columns performed in the plume of Ambrym during the episode of extreme passive degassing
210 the 12th January 2005 (Bani et al., 2009). The measurements were made between 5 and 6h UT
211 onboard of an aircraft flying just below the Ambrym plume (at 500-1000 m above the sea
212 level) in the cross-wind direction (15-40 km south east of the craters) with the instrument's
213 telescope pointing to zenith. The procedure to retrieve the columns is described in Bani et al.
214 (2009) and Bani et al. (2012). Reported errors (2σ) on the SO_2 and BrO retrieved columns are
215 respectively ±52 mg m^{-2} (i.e. 4.89 10^{16} molecules/cm^2) and ±0.39 mg m^{-2} (i.e. 2.44 10^{14}
216 molecules/cm^2). In the present study, these data are used to evaluate the simulation of
217 volcanic plume chemistry. Note that these data in conjunction with wind estimates were used
218 by Bani et al. (2009) to estimate Ambrym SO_2 emission rate (18.8 kt/day).

219

220 **2.2.2 OMI Data**

The Ozone Monitoring instrument (OMI) is a nadir viewing UV/visible CCD spectrometer sampling a swath of 2600 km with a ground footprint of 13 km x 24 km, launched aboard the NASA Aura satellite in July 2004 (Bharthia and Wellemeyer, 2002). Here, we use the planetary boundary layer (PBL) level-2 SO_2 column amount product derived with the principal component analysis (PCA) algorithm (Li et al., 2013). Only data with scenes near the center of the swath (rows 5-55) with radiative cloud fraction less than 0.3 and with ozone slant column lower than 1500 DU were considered as recommended. Noise and biases in retrievals are estimated at ~0.5 DU for regions between 30°S-30°N.

2.2.3 MODIS data

The Moderate Resolution Imaging Spectroradiometer (MODIS) was launched aboard the NASA's Aqua satellite in May 2002. MODIS instrument measures spectral radiances in 36 high spectral resolution bands between 410 to 14400 nm, sampling a swath of 2330 km (Remer et al., 2008). We used the Aerosol Optical depth at 550 nm for both ocean and land product derived from eight-day average of global 1°x 1° gridded daily level-3 products from MODIS/Aqua (MYD08_E3 Collection 5.1). MODIS AOD are derived using algorithms detailed in Remer et al. (2005). Over oceans, MODIS AOD (τ) uncertainties have been shown to be about $\pm$ (0.03 + 0.05τ), over land retrieval uncertainties are generally $\pm$(0.05 + 0.15τ) (Remer et al., 2008). It is important to note that we had to use the eight-day average AOD product because the daily files had too much missing data due to the presence of clouds in the Vanuatu region.

2.3 Model description and simulations

We use the CCATT-BRAMS (Coupled Chemistry Aerosol-Tracer Transport model to the Brazilian developments on the Regional Atmospheric Modeling System, version 4.3) non-hydrostatic regional atmospheric chemistry model (described in detail in Longo et al., 2013). It is based on the Regional Atmospheric Modeling System (RAMS) developed by University

of Colorado for a range of applications: from large eddy simulations in the planetary boundary layer to operational weather forecasting and climate studies (Walko et al., 2000). BRAMS builds upon RAMS and includes modifications and new features to improve the model performances within the tropics (Freitas et al., 2009). The parameterizations of physical processes such as surface-air exchanges, turbulence, convection, radiation and cloud microphysics are described in Freitas et al. (2009) and in Longo et al. (2013). BRAMS is coupled on-line to CCATT that enables transport, chemical evolution, emission and deposition of chemical and aerosol species (Longo et al., 2013). Note that when BRAMS and CCATT are coupled, as in the present study, the prognostic chemical fields, O_3, N_2O, CO_2, CH_4 are used in the radiation scheme. The model has already been used to study regional air pollution, for instance: the South America regional smoke plume (Rosario et al., 2013) and ozone production and transport over the Amazon Basin (Bela et al., 2015). It has also been used to assess the transport of tropospheric tracers by tropical convection (Arteta, 2009a, b) and for understanding the budget of bromoform (Marécal et al., 2012).

The CCATT model is described in detail by Longo et al. (2013). Here we focus on the particular settings of the model we used and the changes we made for the study.

2.3.1 Model Chemistry

Within the CCATT model, we use the RACM chemistry scheme (Regional Atmospheric chemistry Mechanism, Stockwell et al., 1997) including 88 species and 237 chemical reactions and designed to study tropospheric chemistry from urban to remote conditions. Photolysis rates are calculated on-line during the simulation to take into account the presence of aerosols and clouds using Fast-TUV (Tropospheric ultraviolet and visible radiation model, Tie et al., 2003; Longo et al., 2013). The sulfur scheme includes gas-phase oxidation, and dry and wet deposition, but not aqueous-phase oxidation. In order to simulate halogen chemistry

in volcanic plumes, we have added to the chemical scheme 16 halogen species and 54 reactions including photolysis, gas phase and heterogeneous reactions. The gas phase constant rates and photolysis cross-sections are from JPL (Sander et al., 2006) and IUPAC (Atkinson et al. 2007). The heterogeneous reactions include the hydrolysis of $BrONO_2$ and the reaction of HOBr + $X^-_{(aq)}$ + $H^+_{(aq)}$ where X = Br or Cl on sulfate aerosol. They are treated here with reactive uptake formulation (Table 1) with constant uptake coefficient. Ongoing developments are being made to prescribe a variable reactive uptake coefficient for HOBr as function of the underlying gas-aerosol reaction kinetics, building on a recent re-evaluation (Roberts et al., 2014b).

For the heterogeneous reaction of $HOBr_{(g)}$ with $X^-_{(aq)}$ where X = Br or Cl, there is a subsequent inter-conversion between the products Br_2 and BrCl within the aerosols, based on the equilibria (Wang et al., 1994):

E1 $$BrCl_{(aq)} + Br^-_{(aq)} \xleftrightarrow{K_1} Br_2Cl^-_{(aq)}$$

E2 $$Br_2Cl^-_{(aq)} \xleftrightarrow{K_2} Br_{2(aq)} + Cl^-_{(aq)}$$

As a result, the relative amount of Br_2 and BrCl produced and released into the atmosphere depends on the equilibrium established by these two reactions. The Br_2/BrCl ratio is given by E3 (derived from equilibria of Wang et al., 1994):

E3 $$\frac{[Br_{2(aq)}]}{[BrCl_{(aq)}]} = \frac{K_1}{K_2}\frac{[Br^-_{(aq)}]}{[Cl^-_{(aq)}]}$$

where the equilibrium constants of E1 and E2 are $K_1 = 1.8 \cdot 10^4$ M^{-1} and $K_2 = 1.3$ M^{-1} respectively and the amounts of $[Br^-]$ and $[Cl^-]$ in the aqueous phase are determined by the effective Henry's law constants (taken from Sander, 1999). We thus parameterize the reactive uptake coefficient of HOBr as two competing reactions (with Br^- and Cl^-) and, on the basis of

E3, apply a branching ratio to the constant rates of reactions as shown in Table 1. This approach is the same as that proposed by Grellier et al. (2014), and also similar to Roberts et al. (2014a) that showed competition between Br_2 and BrCl as products from HOBr reactive uptake, finding Br_2 is initially formed but BrCl becomes more prevalent once HBr becomes depleted. Note that heterogeneous reactions involving HOCl and $ClONO_2$ are slow compared to the reactions involving HOBr and $BrONO_2$ and are not taken into account in the model.

2.3.2 Sulfate aerosol surface density

In the model, sulphuric acid H_2SO_4 is a prognostic variable and assumed to be in totally in the aerosol phase. It is both directly emitted by the volcano (see section 2.3.3 for details) and produced by the reaction of SO_2 with OH in the gas phase. We assume to have only binary H_2SO_4-H_2O aerosol. Weight percent of H_2SO_4 in the aerosol (wt) and the density of aerosols (ρ_{aer}) are calculated with the analytical expression of Tabazadeh et al. (1997) depending on the temperature and relative humidity. Total volume of aerosol V_{aer} (per cm^3) can then be calculated from H_2SO_4 concentrations, wt and ρ_{aer}. Few observations of volcanic aerosol size distribution exist, and none have been reported for Ambrym volcano plume. We assumed that the aerosols size follows a log-normal distribution with a fixed median diameter (D_{median} = 0.5 μm) and a fixed geometric standard deviation (σ = 1.8). On this basis, the number of aerosol particles was deduced from V_{aer}, D_{median} and σ and the total aerosol surface densities (cm^2/cm^3) was then calculated (further details on lognormal aerosol distributions can be found in Seinfeld and Pandis, 2006). Here, the resulting surface area distribution (Figure 4s) has a surface median diameter of 1 μm and a maximum surface area of 7000 $\mu m^2/cm^3$ in the near-downwind plume. This maximum value corresponds to a surface of 7×10^{-11} μm^2/molec. SO_2^{-1}, a value that lies in the range of order (10^{-11}- 10^{-10} μm^2/molec. SO_2^{-1}) studied by Roberts et al. (2014a). It is also broadly consistent with a recent estimate of aerosol surface area (relative

316 to SO_2) made for Mt Etna (Roberts et al., 2016). Ongoing developments are being made to
317 improve the volcanic aerosol representation to include two modes with diameter varying with
318 hygroscopy, based on recent observations (Roberts et al., 2015).
319
320 **2.3.3 Emissions:**
321 To generate the emissions, we have used the preprocessor PREP_CHEM_SRC (version 4.3)
322 code described in detailed in Freitas et al. (2011). Anthropogenic emissions were prescribed
323 using the RETRO (REanalysis of the TROposhperic chemical composition) global database
324 (Schultz et al., 2007). Fire emissions were estimated using the Global Fire Emissions
325 Database (GFEDv2) with 1°×1° spatial resolution and a 8-day temporal resolution (van der
326 Werf et al., 2006). Biogenic emissions were provided by a monthly mean climatology for the
327 year 2000 produced with the MEGAN (Model of Emissions of Gases and Aerosols from
328 Nature) database (Guenther et al., 2006). Details on the treatment of volcanic emissions and
329 its modification for this study are given in the following.
330 **SO_2 emissions**
331 In CCATT-BRAMS, volcanic SO_2 emission rates are prescribed using the AEROCOM
332 (Aerosol Comparisons between Observation and Models) database (Diehl et al. 2012; Freitas
333 et al., 2011). This database includes volcanoes listed in the Smithsonian Institution's Global
334 Volcanism Program database (GVP) (Siebert et al.; 2010). Their emissions rates are assigned
335 depending on their eruptive state (pre-eruptive, intra-eruptive, post-eruptive and extra-
336 eruptive degassing), on their Volcanic Explosive Index (VEI) in case of eruption, and on
337 additional information from TOMS (Total Ozone Mapping Spectrometer), OMI instruments
338 and COSPEC (Correlation spectrometer) measurements) when available (Diehl et al., 2012).

339 Here, we replaced the values from the AEROCOM database for volcanoes of the Vanuatu Arc
340 by more relevant information, when they were available. In particular, SO_2 emission rate for
341 Ambrym (18.8 kt/day) is reported by Bani et al. (2009, 2012), using DOAS measurements
342 (described in section 2.2.1) in conjunction with wind-speed estimates. The error on this source
343 is about ± 20 % according to Bani et al. (2009).
344 SO_2 emissions rates of the most important volcanoes of the Vanuatu Arc in January 2005 are
345 summarized in Table 2. Note that the Bagana volcano (6.140°S, 155.195°E, alt=1750 m) in
346 Papua New Guinea was also in activity for the period of the simulation, with an emission of
347 3.3 kt/day of SO_2 according to the AEROCOM database.
348 **HBr and HCl emissions**
349 HBr and HCl emission rates are derived from the measurements of HBr, HCl and SO_2 average
350 fluxes reported for Ambrym by Allard et al. (2009). These average fluxes were based on
351 airborne DOAS (to determine SO_2 flux) combined with gas ratios (to SO_2) calculated from
352 crater-rim deployments of filter-pack samplers (for HBr, HCl, HF with SO_2) and Multi-Gas
353 sensors (for CO_2, H_2O with SO_2), and are representative of a mean volcanic emission of
354 Ambrym (Allard, personal communication). We did not use directly the HBr and HCl
355 measurements but instead derived the HBr/SO_2 and HCl/SO_2 mass ratios ($8.75 \cdot 10^{-4}$ and 0.1,
356 respectively) from the reported fluxes and applied them to our January 2005 SO_2 emission
357 rate value to estimate the HBr and HCl emissions specifically for this date. Indeed, volcanic
358 emission fluxes can vary with time. Allard et al. (2009) reported mean SO_2 emission rate for
359 instance totals 8.8 kt/day, about two times smaller than the SO_2 emission rate reported during
360 the extreme passive degassing event of 18.8 kt/day, but in closer agreement with the estimate
361 by Bani et al. (2012) of Ambrym mean activity of 5.4 kt/day for the period 2004-2009. The
362 calculation yields HCl and HBr emissions of 1.9 kt/day and 16.5 t/day. Of note, the HBr/SO_2
363 and HCl/SO_2 mass ratios are close to (for HBr/SO_2 perhaps somewhat higher) mean estimates

for volcanic degassing as reported by Pyle and Mather (2009), but due to the high Ambrym SO_2 flux they yield very high volcanic halogen fluxes. By comparison, the Br flux from Mt Etna is reported as only 0.7 kt/yr (Aiuppa et al., 2005) i.e. 1.9 t/day, almost 10 times smaller. Note also that HF emissions were not considered in this study: whilst deposition impacts from HF around Ambrym can be severe (Allibone et al. 2010), HF does not contribute to reactive halogen cycling in the atmosphere (prevented by the strong H-F bond).

Sulfate emissions

We assume that 1% of the sulphur (= SO_2 + H_2SO_4 here) is emitted as H_2SO_4 aerosol based on reported observations from several filter-pack studies at different volcanoes worldwide (e.g., Mather et al., 2003, Von Glasow et al., 2009 and references therein).

Initialisation with output from HSC Chemistry thermodynamic model

As mentioned earlier (see Section 1), the mixing of volcanic gas with ambient air at the vent leads to high temperature oxidative dissociation processes and hence to the formation of radical species. To take into account this high temperature chemistry, the thermodynamic model HSC Chemistry (Roine, 2007) was applied to simulate the equilibrium chemical composition of the volcanic gas-air mixture assuming a 98:2 volcanic gas:atmospheric gas composition. This approach follows that of previous 1D model studies (Bobrowski et al.., 2007, Roberts et al., 2009, Von Glasow 2010, Kelly et al., 2013, Roberts et al., 2014a, Surl et al., 2015). The model temperature was based on mixing an atmospheric temperature of 20 ˚C (consistent with that predicted by the CCATT-BRAMS model) and the magmatic degassing temperature of 1125 ˚C estimated by Sheehan and Barclay (2015). This was based on calculation of crystallisation temperatures of mineral phases in scoria samples collected from Ambrym in 2005, following models of Putirka (2008). The HSC Chemistry model input composition, shown in Table 3, is a 98:2 mixture of magmatic gases (with composition based on Allard et al., 2009), and atmospheric gases (78% N_2, 21% O_2, 1% Ar). Roberts et al.

389 (2014a) identifies key new species in the HSC Chemistry output as Br, Cl, OH and NO.
390 Fluxes of these species were calculated from their ratio to sulphur in the HSC Chemistry
391 output, and by scaling with the (prescribed) SO_2 flux in the CCATT-BRAMS model. Due to
392 uncertainty in volcanic NO_x emissions (see discussions of Martin et al., 2012; Roberts et al.,
393 2014a; Surl et al., 2015), HSC Chemistry outputs both with and without NO_x were used to
394 initialise CCATT-BRAMS (Simulations S1_HighT and S1_HighT_noNOx). Note that the
395 HSC output also contains SO_3, which is the precursor to volcanic sulfate. However, as
396 mentioned above, in this study the volcanic sulfate emission was instead fixed to 1% (by
397 mole) of sulfur in all runs. All the emissions for the different simulations are summarized in
398 Table 4.

399 **Plume height**

400 The information on plume heights is from AEROCOM database and from Bani et al. (2012).
401 They give respectively plume heights of 1373 m and of 2000 m (in our study, all the altitudes
402 are above sea level unless otherwise mentioned). Note that the mean altitude of both crater
403 rims is about 1000 m. Bani et al. (2012) report an altitude of the plume of 2000 m for the
404 degassing event of 12th of January 2005 that was estimated visually. For the other periods,
405 their estimation of the altitude varies between 700 m (i.e. below the craters) and 2000 m. For
406 the case study of the degassing event of January 2005, it was not clear to us from videos and
407 pictures that the plume altitude was about 2000 m. As a result, we performed a sensitivity
408 study on the plume height (see Supplementary Material). In a first simulation, emissions are
409 injected in the model box vertically above the volcano that includes the 1373 m altitude point.
410 This model box is not the same in each grid, as the topography depends on the grid resolution.
411 As a result, its depth varies between about 100-200 m. In a second simulation, emissions are
412 injected higher up in the box containing the 2000 m altitude, whose depth varies between
413 about 200-300m. As shown later, we performed an additional sensitivity analysis, where the

emissions are this time spread over two vertically adjacent grid boxes (section 3.3.1). The depth of the plume in the model this time is about 300 m to 400 m. Figure 1 shows the distribution of volcanic emissions in the vertical prescribed in the model for the different sensitivity simulations.

2.3.4 Model general set-up and simulations

In our study, the primary horizontal resolution is 50 km × 50 km with 44 vertical levels from the ground to 27 km. Three nested grids (10 km × 10km, 2 km × 2 km and 0.5 km × 0.5 km) was also added. Model domain and grids are shown in Figure 2. Horizontal winds, geopotential height, air temperature and water vapor mixing ratios from ECMWF analysis (with a 0.5° × 0.5° resolution) are used to initialize and nudge the model using a four dimensional data assimilation (4DDA) technique with a relaxation time constant ranging from 30 min at the lateral boundaries to 6 hours at the center of the domain. Initial and boundary conditions for concentrations of the chemical species were provided by 6-hourly output from the global chemical transport model MOCAGE (Josse et al., 2004) with a resolution of 1° × 1°.

In the following, we describe the different simulations performed in this study. All the simulations start the 1st of January 2005 00:00 UTC with the larger grid only. As this was an extreme degassing event of long duration (several months) rather than an episodic eruption, the model initialization from 1st January 2005 already includes the Ambrym emissions. Due to computing limitations, the 3 nested grids are only added the 11th of January 2005 00:00 UTC with the initial conditions given by the corresponding simulation with one grid. The different simulations differ in terms of the strength of the emissions, the nature of the emitted compounds and the repartition of the emissions in the vertical. They are summarized below, as well as in Table 4 and Figure 1:

- S1 includes the standard volcanic emissions (SO_2, H_2SO_4, HCl, HBr).

- S1_HighT includes emissions (SO_2, H_2SO_4, HCl, HBr, OH, NO, Cl, Br) derived from an HSC Chemistry simulation described in section 2.3.4.4 and in Table 3.

- S0 has the same emissions as S1_HighT except that emissions from Ambrym volcano have been turned off.

- S1_HighT_alt simulation is exactly the same as S1_HighT except that the height of plume is fixed to 2000m.

- S1_HighT_width is exactly the same than S1_HighT except that the plume of Ambrym spans two grid boxes (in the vertical) instead of one.

- S1_HighT_noNOx simulation is exactly the same than S1_HighT except that emissions of NO have been turned off.

- S1_nohal has the same emissions as S1_HighT except that Ambrym volcano includes only SO_2 emissions.

- S1_nohal2 has the same emissions as S1_HighT except that Ambrym volcano includes only SO_2 emissions and the same emissions of OH than S1_HighT.

- S1_HighT_surf is exactly the same than S1_HighT except area surface density was increased by a factor of 10.

In the next section, we evaluate the performances of the model CCATT-BRAMS to simulate near downwind volcanic plume chemistry for the Ambrym extreme passive degassing of 12th January 2005 using the airborne DOAS observations of SO_2 and BrO columns and in the context of previous work.

3. Analysis of the modeled volcanic chemistry in the near downwind plume

3.1 Evaluation of the modeled SO_2 and BrO columns amounts in the near downwind plume

463 Figure 3 shows the SO_2 columns amounts observed during 4 traverses of the near downwind
464 Ambrym plume (between 15 to 40 km of the vent) on 12th January 2005 between 05:00 and
465 06:00 UTC (Bani et al. 2009; 2012) and the corresponding SO_2 columns amounts simulated
466 by the model for the S1 (i.e. including the standard emission) and S1_HighT (i.e. initialized
467 with the output of the HSC Chemistry model as described in Section 2.3.3) on the grid 0.5 km
468 × 0.5 km (see section 2.3.4 for the description of the simulations). Statistical quantities (mean,
469 RMS, correlation) were calculated to compare more quantitatively observations and
470 simulations (Table 5). Note that sensitivity studies to the height of the plume and the vertical
471 extent of the plume will be discussed further in section 3.3.

472 **3.1.1 SO_2 columns**

473 Observations show that SO_2 columns decrease with distance from the vent and exhibit a
474 bimodal distribution across the plume. Each mode is attributed by Bani et al. (2009) to the
475 individual plume of the two degassing craters Benbow and Marum that are situated 3km
476 apart. Figure 3 shows that the model captures relatively well the magnitude of the SO_2
477 columns along and across the plume for the S1 and S1_HighT simulations. The mean
478 difference between observations and simulations is lower than 2% (relatively to the mean of
479 the observation) and the correlation coefficient is about 0.6 (Table 5). However, we can note
480 that the influence of the 2 craters Benbow and Marum is not seen as clearly as in the
481 observations. This suggests a limitation linked to the model resolution, even though the model
482 resolution for the particular grid shown is 500 m × 500 m. We can also note that the simulated
483 plume tends to be slightly titled eastward compared to the observations in particular for the
484 transects at 20 km and 21 km (not shown) from the vent but to a lesser extent for the transect
485 at 40 km. This is the reason for the relatively high RMS values (about 50 % of the mean SO_2,
486 see Table 5) but it does not affect the bias (2%).

Previous work at volcanoes elsewhere (e.g., Bobrowski et al., 2007) reported that the observed SO_2 variations in the near downwind plume are almost exclusively due to plume dilution. As a test, we have included in our simulation an SO_2 "tracer" whose emission and deposition are the same as for SO_2 but whose chemical loss is equal to zero. We find that the difference between the SO_2 columns field and the SO_2 tracer columns field at a distance of 40 km from the vent is less than 0.5 % (not shown), confirming that the SO_2 decrease in the model with distance from the vent in Figure 3 is mostly due to plume dilution. Therefore, we can conclude from the comparison in Figure 3 that the direction of the plume as well as its dilution are reasonably well simulated by the model in the simulations S1 and S1_HighT. It is important to note that we cannot conclude here on the strength of the Ambrym SO_2 source. Indeed, our rational would be circular as we have used in our model the SO_2 source strength (described in Section 2.3.3.1 and Table 2) which Bani et al. (2009, 2012) derived from the same DOAS data (combined with winds estimates) used here for the model evaluation. Note also that we performed a simulation S1_HighT_alt, similar to S1_HighT except that the plume height was 2000 m as reported by Bani et al. (2012). We find that the simulation S1_HighT_alt (see supplementary material section 1 as well as Figures 1S and 2S for more detail) underestimates the observations by 44 % for SO_2 (compared to 2% for S1_HighT). The correlation between simulated and observed SO_2 is also reduced, 0.37 (compared to 0.61 for S1_HSC). Given better agreement between the model and observations at the lower injection altitude estimate of ~1400 m, this injection height of S1_HighT was used in the following.

3.1.2 BrO columns

In Figure 4, the same comparison as for Figure 3 is presented for BrO columns amounts. BrO columns, as those of SO_2, decline between 15 and 40 km from a mean of 9.8×10^{14}

512 molecule/cm^2 to a mean 3.2×10^{14} molecule/cm^2. Values as high of 1.8×10^{15} molecule/cm^2 at
513 15 km were reported by Bani et al. (2009). Note that these values are particularly high
514 compared to other BrO column observations at volcanoes elsewhere for which maximal
515 values lie between 10^{14} molecule/cm^2 to 10^{15} molecule/cm^2 (Boichu et al., 2011). Note also
516 that the influences of the two crater sources (Benbow and Marum) are still visible in the BrO
517 data as two distinct peaks.
518 In the standard simulation, the trend in BrO with distance from the vent is reversed compared
519 to the observations (also shown by the negative correlation coefficient of Table 5 of -0.21). At
520 15-20 km downwind from the vents where observed BrO columns are highest, the model (S1)
521 underestimates the mean BrO columns by a factor of 10. Overall, the mean difference
522 between BrO columns observed and those simulated in S1 is about 80 % (Table 5). For the
523 simulation initialized with HSC Chemistry model, the trend in BrO with distance from the
524 crater is in better agreement with the observations (Figure 4 and correlation coefficient of
525 Table 5 of 0.6). An improved overall agreement between model and observations is also
526 found (as seen in Figure 4 and Table 5): the mean bias between observed and simulated BrO
527 columns is about 40% (relative to the mean observations). It is important to note that the bias
528 is more pronounced near source: it varies from 60 % for the transect at 15 km to 14 % for the
529 one at 40 km of the vents.
530 Figure 5 shows the evolution of BrO/SO_2 with distance from the vent derived from the
531 observations and from the simulations presented in Figure 3 and 4. Because SO_2 can be
532 considered as a passive tracer over short timescales, any increase or decrease in BrO/SO_2
533 implies respectively a production or a destruction of BrO. Measurements suggest that BrO
534 formation has occurred and has reached its maximal amount between 0 and 17 km of the vent.
535 Further downwind, between 17 km and 40 km, measurements predict a destruction of BrO. In
536 the simulation initialized with the HSC Chemistry model, the trend in BrO/SO_2 is close to that

observed. The formation of BrO reaches a maximum around 17 km with a plateau between 17 and 21 km and is destroyed between 20-21 and 40 km. In contrast, in the case of the standard simulation S1, BrO builds up between 15 and 40 km. Overall, we conclude that BrO formation is too slow in the standard simulation compared to the observations. On the contrary, the kinetics of BrO formation predicted in the simulation initialized with HSC Chemistry model is in good agreement with the observations. This confirms previous 1D model work that showed the need for radicals to "kick off" the chemistry i.e. accelerate the onset of the chemistry (e.g., Bobrowski et al., 2007; Roberts et al., 2009). In addition, Figure 5 shows that, for each transect, the variability of BrO/SO_2 ratios in the observations and in the S1_HighT simulation have a similar magnitude. In particular, we find that for each transect the model simulates the highest value of the BrO/SO_2 ratio at the edges of the plume as shown in the observations, i.e. for lowest values of SO_2 columns. This result is again consistent with previous work (e.g., Bobrowski et al., 2007; Von Glasow et al. 2009; von Glasow, 2010; Roberts et al., 2014a). At the edges of the plume, more mixing with entrained background air occurs. This leads to higher ozone concentrations and favors BrO (see section 2.1.2). In general, the trends in BrO/SO_2 with distance downwind and between core and plume edge reflect the net impact of a dynamic chemistry involving many reactive bromine chemistry species. In the following section, we analyze in more detail the simulation of volcanic plume chemistry.

3.2 Simulated plume chemistry

Figure 6 shows distance-pressure cross sections of SO_2, OH, HBr, BrO, O_3 and NO_x mixing ratios in the plume of the standard simulation for the 12th of January 2005 at 6 UT (time of the DOAS measurements) in the grid 2 km × 2 km. This grid allows us to visualize the results as far as 200 km downwind. Figure 7 shows the Br speciation among the bromine species

562 along the plume (in the core and at the edges) for the same simulation in the same grid and at
563 the same time. Figure 6 shows that OH is totally depleted in the core of the plume in the
564 simulation. This is due to the elevated concentrations of SO_2 as well as being a consequence
565 of the halogen chemistry (see section 4.4), and mirrors findings from previous 1D model
566 studies (e.g., Roberts et al., 2009, 14a; Von Glasow, 2010). However, as noted before, the
567 decrease of SO_2 along the plume as far as 200 km is mainly due to dilution of the plume.
568 Figures 6 and 7 show that HBr is converted into reactive bromine in the volcanic plume, as
569 expected. However, at about 50 km of the vent, only 20% of this conversion had occurred (80
570 % HBr remains). Indeed, the chemical cycle responsible for HBr conversion is autocalytic so
571 it needs reactive bromine to be initiated. In the standard simulation, the onset of BrO
572 formation is slow because reactive bromine is initially formed by the reaction of HBr with
573 OH, which is slow because OH is depleted. In Figure 6, the enhancement of BrO (and of Br_2
574 in Figure 7) as well as the depletion of O_3, NO_x and HO_x (not shown) confirm that the
575 autocatalytic cycle responsible for HBr conversion to reactive bromine is ongoing in the
576 simulations (see section 2.1.2). Very quickly, in the core of the plume, BrO becomes the
577 dominant species after HBr. Its mixing ratio increases with distance from the vent reaching a
578 maximum of 120 pptv at about 70 km (Figure 6) equivalent to 20% of the total bromine
579 (Figure 7). The depletion of ozone reaches its maximum of 15 ppbv loss (100%) at 70 km,
580 corresponding to the maximum of BrO. Further downwind, Br is the dominant species
581 because O_3, HO_x and NO_x are depleted. In contrast, at the edges of the plume, BrO is still
582 increasing and dominates because more ozone is available than in the core of the plume
583 enabling its formation from Br (R3). Further downwind at the edges of the plume, the
584 formation of BrO slows but does not stop (as shown by the non-zero Br_2 and BrCl fraction) as
585 the plume disperses and dilutes the volcanic aerosol. A dynamic equilibrium is established

586 between BrO, Br and HOBr. We can note that the BrO mixing ratio remains as high as 60
587 pptv at the edge of plume around 200 km downwind (Figure 6).
588 As expected, in the simulation initialized with HSC Chemistry model, the conversion of HBr
589 into reactive bromine is accelerated by the presence of the radical species (Figure 8 and 9).
590 Indeed, the HBr fraction is only 20 % at 25 km from the vent and is almost zero around 30 km
591 downwind at the edge of the plume. Once HBr becomes depleted, a peak of BrCl is observed
592 because the aqueous phase equilibria between BrCl and Br_2 favor BrCl instead of Br_2. Figure
593 8 shows that BrO reaches its maximum earlier, around 15-20 km downwind, than for the
594 standard simulation (70 km), at a distance where the plume is more concentrated. As a result,
595 the maximum of BrO mixing ratios is higher (around 240-260 pptv) than for the standard
596 simulation. Ozone is also entirely depleted in this simulation, it reaches 15 ppbv loss (100 %)
597 around 15 km. In the core of the downwind plume Br becomes the dominant species (up to
598 80 % of Bry, Figure 9) due to this total ozone depletion with ongoing ozone loss processes
599 exceeding any source from entrainment of (ozone-containing) background air into the plume
600 core. HBr can reform by the reaction of Br with HCHO for instance because of the high
601 concentrations of Br in the core of the plume. Further downwind, HBr is then slightly
602 reconverted into BrO, likely because a somewhat enhanced entrainment of ambient air occurs.
603 At the edges of the plume, the chemical cycles are not limited by lack of (background)
604 oxidants. As a result, HBr can be fully consumed and BrO is the dominant species. Further
605 downwind, the formation of ongoing reactive halogen chemistry results in a dynamic
606 equilibrium being established between BrO, Br and HOBr. We can also note that even further
607 downwind (approximately from 150 km from the vent), there is no significant difference
608 between S1 and S1_HighT in terms of absolute concentration of the bromine species and in
609 terms of partitioning among the bromine species.

610 To conclude, the kinetics of BrO formation predicted in the simulation initialized with HSC
611 Chemistry model is in good agreement with the observations. This leads to higher BrO
612 concentrations in near downwind plume and hence to a better comparison with DOAS data.
613 Despite the better comparison between DOAS and S1_HighT, the model still underestimates
614 by 60 % the BrO columns in the near-source plume (at 15 km from the vents). We find that it
615 is due to the ozone depletion in the core of the plume that limits the formation of BrO from
616 Br. In strong (i.e. near-source and under high emissions) volcanic plumes, gas-phase cycling
617 between Br and BrO (reactions, 3, 4a and 4b) is particularly intense. As a consequence, in the
618 core of the plume where the mixing with background ozone is limited, ozone is totally
619 depleted. This lack of ozone limits the partitioning of BrO from Br and hence BrO
620 concentrations.

621 As presented in section 2.3, we had to make some assumptions in our study because of the
622 lack of information to constrain the model or technical limitations. In the next section, we test
623 whether the uncertainties in the representation of some of the crucial processes could affect
624 the model results and explain the discrepancies found between simulations and observations
625 for the closest transects (~15-20 km) from the vents. More specifically, we focus on the depth
626 of the plume that controls the degree of mixing between emissions and background air, the
627 formation of NO_x by the high temperature chemistry and the surface aerosol area that can
628 affect the in-plume chemistry.

629

630 **3.3 Sensitivity studies**

631 **3.3.1 Vertical depth of the plume**.

632 A suggested in section 3.2, BrO formation appears to be limited by ozone concentrations in
633 the simulation S1_HighT. However, values of background ozone in the model seem in good

agreement with ozone climatology (e.g., Logan et al., 1999) that indicates ozone mixing ratios of 15-20 ppbv below 800 hPa in the Pacific region. Here in an attempt to avoid the limitation of BrO formation due to lack of ozone, we have increased the degree of the mixing between the emissions and the background air in the vertical. Practically, we have artificially increased the vertical depth of the plume by spreading out the emissions over two vertically adjacent levels (see Figure 1). More specifically, in the simulation S1_HighT_width, the emissions were distributed equally between the vertical grid box of the S1_HighT simulation and the one just above. As a result, the Br molecules are exposed to roughly twice as many ozone molecules. Note that we did not change the degree of mixing in the horizontal because Figure 3, showing the comparison of SO_2 columns distribution across the plume, seems to indicate that the width of the plume at different distances from the vents is reasonably well simulated by the model.

We find that the comparison with DOAS for SO_2 does not improve (mean bias of 17 % and a correlation of 0.55, Figure 1S). Concerning BrO, our results are very similar to those obtained with S1_HighT (slightly worse with mean bias of 43% and with a correlation coefficient of 0.54, Figure 2S). The weak impact of this sensitivity study can be explained by the fact that the vertical diffusion in the model has already dispersed very quickly the emissions through several vertical levels in S1_HighT. Thus, BrO formation is already limited by ozone in the upper level where the emission was additionally injected in S1_HighT_width. As a result, we have tried different combinations to spread out the emissions over more than 2 levels in the vertical between the level of injection of S1_HighT (~1400 m) and the level of injection of S1_HighT_alt (~2000 m) (see Figure1). But, the wind direction changes with the altitude between these two levels in our simulations. Therefore, the comparison of SO_2 columns distribution across the plume, that was fairly good for S1_HighT, worsens in these model runsand tends to become very similar to the one obtained with S1_HighT_alt (see Figure 1s).

3.3.2 Formation of NO_x by high temperature chemistry

There are numerous uncertainties concerning the high temperature chemistry taking place in the mixture of volcanic gases and ambient air at the vent (Martin et al., 2009; 2012). In particular, models used to calculate this chemistry assume thermodynamic equilibrium. However, Martin et al. (2012) calculated that the thermal N_2 fixation is too slow for equilibrium to be attained at volcanic vents. Hence, the production of NO_x by the HSC model could be overestimated. Conversely, volcanic NO_x production is suggested by several observations of NO, NO_2, HNO_3, HO_2NO_2 in the near-source plume (e.g., Mather et al. 2004; Oppenheimer et al., 2010; Martin et al., 2012, Voigt et al., 2014), with NO_x to HNO_3 conversion pathway proposed by Roberts et al. (2009, 2014a). In the case of Ambrym, no information is available on the absence or presence of volcanic NO_x, nor other reactive nitrogen species in the plume. We performed a simulation (S1_HighT_noNO_X) where NO_x from the high-temperature initialization was not included while keeping constant the emissions of the other radicals (i.e. OH, Cl, Br) from HSC Chemistry. In this case, the SO_2 field is exactly the same as in S1_HighT (Figure 1S). The comparison between BrO in S1_HighT_noNO_X and the observations (Figure 2S) is very close to what is obtained for S1_HighT (mean model observation difference is about 44% and the correlation is about 0.63). Figure 3S gives some explanation for this. It shows that the kinetics of HBr conversion in S1_HighT_noNO_X is similar to that in S1_HighT in the first 10-15 km from the vent and it is much slower after 15 km. This suggests that NO_x emissions are not crucial to kick off the plume chemistry initially but that they are responsible for the decline of HBr further downwind after 15 km. This delayed role of the NOx radicals was also found in 1D model study presented by Roberts et al. (2009) (see their figure 4). In our case, this is further confirmed by Figure 8 where it can be seen that NO_x depletion in S1_HighT starts after 10-15 km. The role of NO_x is linked to the formation of $BrONO_2$ from BrO and NO_2 followed by its

684 rapid hydrolysis on volcanic sulfate aerosol that acts to convert BrO into HOBr and that can
685 then undergo another heterogeneous chemical cycle to release reactive bromine from HBr ($Br^-_{(aq)}$).
686 Without NO_x, this conversion of BrO into HOBr depends on the presence of HO_2 via the
687 reaction of BrO with HO_2. Note also that due to the slower decrease of HBr in
688 S1_HighT_noNOX after 10-15 km, no BrCl peak is visible in Figure 3S in the near
689 downwind in contrast to Figure 9 for the S1_HighT simulation. To conclude, the difference in
690 BrO kinetics in S1_HighT and S1_HighT_noNOx is mostly visible after 10-15 km from the
691 vent. Hence, it does not impact the initial near-downwind rise in BrO. This contrasts with the
692 model studies of Von Glasow (2010) and Surl et al. (2015) for Mt Etna who suggested a
693 volcanic NO_x emission acts to lower plume BrO due to the formation of $BrNO_2$ that persists in
694 the plume. However, Roberts et al. (2014a) highlighted additional pathways for $BrNO_2$
695 removal enabling regeneration of BrO. Given uncertainties in the chemistry, $BrNO_2$ is not
696 included in our study.
697 To conclude, the simulations S1_HighT and S1_HighT_noNOx exhibit similar kinetics of
698 BrO formation and also a similar magnitude in the BrO maximum. As a result, uncertainty in
699 the presence of volcanic NO_x in the emission cannot explain the discrepancy between the
700 model and reported downwind plume BrO. In addition, we can also note that the BrO and
701 SO_2 columns measurements alone are not sufficient to fully constrain the parameter space of
702 our modeling of volcanic plume chemistry. In particular, NO_x and HNO_3/nitrate should be
703 measured in volcanic plumes to constrain the reactive nitrogen emission.

704 **3.3.3 Sulfate aerosol surface density**

705 Despite a broad agreement with previous estimates (see section 2.3.2), aerosol surface density
706 remains a source of uncertainty in our study our as we do not have direct measurements of
707 aerosols for Ambrym. Therefore we have increased the sulfate aerosol surface density by a
708 factor 10, still keeping the value in the right range of order (section 2.3.2), to test whether this

uncertainty could explain the pronounced discrepancy on BrO columns near-source. We would expect that an increased aerosol surface area would increase the conversion of HBr into reactive bromine and hence the concentrations of BrO. Note, that this sensitivity study is equivalent to increase the HOBr reactive uptake coefficient on sulfate aerosols, for which large uncertainties exist (see Roberts et al., 2014a), while keeping constant the aerosol surface area. We find that our sensitivity study impacts only very slightly the value of near-source BrO columns (bias of 62 % compared to the bias of 60% for S1_HighT). Indeed, BrO is determined by the partitioning with Br mainly by reactions R3, R4a and R4b in the concentrated plume. Because ozone is quickly consumed, the formation of BrO is limited as discussed earlier. This is also in agreement with the sensitivity studies performed with the PlumeChem model (Roberts et al. 2014a) for Mt Etna where increasing the aerosols surface density by a factor 10 increased only slightly the BrO/SO_2 ratio in the near downwind plume. Note that we did not test the sensitivity of the model results to the strength of total bromine emissions. Increasing total bromine emissions would increase total bromine in the plume. But because of the ozone limitation, this would lead to a reduced fraction of BrO and increased fraction of Br. Finally, these two effects would compensate as found with a 1D model for the Nyiragongo's plume by Bobrowski et al. (2015). As a result, increasing total bromine emissions would not impact BrO columns. This compensation was also found by Roberts et al. (2014) with their 1D model when compared their "high" and "medium" total bromine scenarios.

To conclude, the uncertainties on plume depth, NO_x emissions, aerosol loading as well as injection height cannot explain the discrepancy between the model and the reported near source BrO. Instead, we find that BrO formation is ozone limited in our model runs. This is also found in the model 1D runs of Bobrowski et al. (2015) of the Nyiragongo's plume, who conclude that measurement of ozone should be a priority for next measurements campaigns.

More generally, BrO and SO_2 columns measurements are not sufficient to constrain the modeling of volcanic plume chemistry as also highlighted in Bobrowski et al. (2015). It is also important to note that the discrepancy between simulated and measured BrO columns remains limited to the near downwind plume. Indeed, the modeled BrO columns agree within 14 % with the farthest observations (~40 km of the vents). As the result, this discrepancy does not significantly impair the analysis of the regional impact of Ambrym presented below.

4 Regional impact of Ambrym volcanic emissions

4.1 Evaluation of the plume simulation at the regional scale with OMI

Figure 10 shows SO_2 columns on 12th of January 2005 at 02:30 UT from OMI and the corresponding SO_2 columns interpolated on the OMI grid from CCATT-BRAMS. The model result is for the grid resolution of 10 km × 10 km that is of similar size to the OMI data (13 km × 24 km). At this time of the year, the plumes from Marum and Benbow are generally carried to the northwest by the trade winds. As shown, in Figure 10, on January 12th 2005, they were carried to the south, because of the influence of the Cyclone Kerry, located around 1800 km southwest of Vanuatu (Bani et al., 2009). Figure 10 suggests that the direction of the plume is correctly simulated at the regional scale. To quantify the degree of spatial matching between modeled and observed SO_2 plumes, we have calculated the Figure of Merit in Space (FMS) which is the ratio between the intersection of the observed and simulated plumes areas and their union (Mosca et al., 1998). Using a threshold of 5×10^{16} molec. SO_2/cm^2 to define the Ambrym plume in both OMI and model fields, we find a FMS of 62% that suggests a fairly good spatial agreement between observed and modeled plumes. The difference between observed and simulated SO_2 columns distributions is mainly due to the plume width that is slightly larger in the simulations than in OMI data (Figure 10). The magnitudes of the mean columns in both plumes match also fairly well: the mean difference is about 25 % (relative to the observations). This difference is due to the presence of some SO_2 enhancements in the

759 plume in the OMI data that are not seen in the simulations. Note that the truncated length of
760 the SO_2 plume in the OMI data is related to the presence of clouds north east of New
761 Caledonia. It is important to notice that the present comparison also shows that simulated SO_2
762 columns, when initialized with the Ambrym SO_2 source strength estimate derived from the
763 DOAS observations by Bani et al. (2009) and (2012), agree within 25 % to the SO_2 columns
764 detected by OMI.
765

766 **4.2 Impact of Ambrym on sulfate, bromine and ozone at the regional scale**

767 Our simulations include 4 grids. To study impacts of Ambrym at the regional scale, model
768 outputs for the largest grid (see Figure 2), whose resolution is 50 km x 50 km, are analyzed.
769 Because of computing limitations, we present only the impact for the 12th January 2005 after
770 11 days of spin-up.

771 **4.2.1 Sulfate**

772 The sulfate burden in the model domain due to Ambrym increases by 44% (i.e. 0.08 Tg of
773 sulfate) value calculated as the mean difference in sulfate between S1_HighT and S0 for 12th
774 January. The direct sulfate emission totals 3.34 Gg of sulfate since the beginning of the
775 simulation. This means that at least 96 % (≈ (80-3.34)/80 x100) of the sulfate burden increase
776 due to Ambrym results from atmospheric oxidation of SO_2 from the volcano by OH. It is a
777 lower limit as direct emissions could have left the domain during the simulation or have
778 undergone deposition. Thus we confirm that sulfate formed from atmospheric oxidation of
779 SO_2 is the dominant driver of the plume halogen chemistry on the regional scale. This
780 contrasts to the near-downwind plume where the directly emitted sulfate (formed from high-
781 temperature SO_3) is dominant and is essential for the rapid formation of BrO (see Roberts et
782 al., 2009, von Glasow, 2010).

783 Figure 11 shows the spatial distribution of sulfate due to Ambrym emissions calculated as the
784 daily mean difference between the simulation S1_HighT and S0 for 12th January 2005. The
785 vertical profile of this daily averaged (across the domain) sulfate is also shown in Figure 12
786 for S1_HighT and S0 simulations. This Figure shows that the contribution of Ambrym to the
787 sulfate in the domain is mostly confined below 600 hPa. Figure 11 indicates that it can reach
788 2.5 ppbv in the plume at 875 hPa, the approximate altitude of the emissions injection in the
789 simulation. The contribution of Ambrym is also particularly high (hundreds of pptv) in an
790 extensive zone west of the volcano at 875 hPa. In the middle troposphere (500 hPa) and in the
791 Tropical Tropopause Layer (150 hPa), the influence of Ambrym is more localized. It is co-
792 localized with convective events as can be seen in the precipitation data of the TRMM
793 (Tropical Rainfall Measuring Mission) satellite (Huffman et al., 2007) and simulated by the
794 model (Figure 13). More precisely, the 500 hPa enhancement is co-localized with a band of
795 convective systems situated south east of New Caledonia the 12th and in the days prior. This is
796 further confirmed by the analysis of forward trajectories initialized from Ambrym on the 10th
797 and 11th of January 2005 (Figure 14) calculated with the HYSPLIT transport and dispersion
798 model (Draxler and Rolph, 2003). The enhancement of sulfate at 150 hPa is co-localized with
799 a convective event that happened north of Vanuatu on the 11th as suggested by the TRMM
800 data (not shown) and could also result from transport from a convective event that occurred to
801 the south as shown in Figure 13. These localized enhancements of sulfate in the middle and
802 upper troposphere due to Ambrym can reach 700 pptv at 500 hPa and 250 pptv at 150 hPa.
803 Overall, over the whole domain, above 600 hPa, the influence of Ambrym emissions is
804 reduced: sulfate mixing ratios are increased by 30 pptv for example at 300hPa. This is
805 explained by the fact that sulfate aerosols are strongly washed-out by precipitation in the
806 model. In this model study, the aqueous-phase oxidation of SO_2 to sulfate was not taken into
807 account. This process becomes self-limiting in strong volcanic plumes due to the titration of

808 oxidants for example H_2O_2 (Schmidt et al., 2010) but may have a significant contribution to
809 sulfate formation over the whole model domain, especially because the region studied is
810 particularly cloudy as shown by Figure 13. Thus this will be considered in future work.
811 Total aerosol optical depth (AOD) at 550 nm from MODIS/Aqua is also shown in Figure 5s
812 of supplementary material for the 9-16 January 2005. Enhanced AOD are clearly seen
813 southeast of Ambrym in the direction taken by the plume the 12th January 2005 as discussed
814 earlier (see Figure10) as well as northwest of Ambrym in the direction of trades winds. The
815 latter point is again consistent with OMI SO2 images from GSFC (Goddard Space Flight
816 Center) at http://so2.gsfc.nasa.gov/pix/daily/0105/vanuatu_0105z.html) showing that the
817 plume was carried toward the northwest on the 14th and 15th January 2005. Figure 5s shows
818 that enhanced AOD values varies between 0.12 and 0.34, which are approximately twice
819 higher than the 3 years average (Oct.2005-Oct.2008) AOD from MODIS presented by
820 Lefevre at al. (2015). This is consistent with the extreme passive degassing activity of
821 Ambrym during January 2005. This confirms the strong influence of Ambrym on the budget
822 of sulfate aerosol in the South West Pacific region and is qualitatively in agreement with our
823 results.
824 **4.2.2 Bromine**
825 Figure 15 shows the horizontal distribution of the total bromine content (Br_y= HBr + $2Br_2$ +
826 BrCl+ Br + BrO + HOBr + $BrONO_2$) due to Ambrym emissions calculated as the daily mean
827 difference between the simulation S1_HighT and S0 for 12th January 2005. The vertical
828 profile of this daily averaged Br_y is shown in Figure 16 for S1_HighT and S0 simulations.
829 The results presented here are for the larger grid whose resolution is 50 km × 50 km. The
830 regional influence of Ambrym volcano emissions as a source of Br_y is clearly demonstrated.
831 Ambrym is the main volcanic source of bromine in the domain, causing a regional plume of
832 enhanced Br_y (maximum of 60 pptv) in the lower troposphere. Bagana volcano in Papua New

833 Guinea was also active at this time (see section 2.3.3.1), and is responsible for a smaller
834 enhancement in the S0 simulation around 875 hPa seen in Figure 16. In the middle
835 troposphere (500 hPa) and in the Tropical Tropopause Layer (150 hPa), the influence of
836 Ambrym is still visible but more localized, increasing locally the background Br_y by up to 3
837 pptv. The same convective events as those mentioned in the previous section are responsible
838 for these Br_y enhancements. There is also evidence of transport to the stratosphere when
839 analysing results at 80 hPa (a model level that is above the thermal tropopause in the
840 simulation) with a few visible patches of Br_y of up to 0.5 pptv. Such transport of volcanic
841 bromine to the upper troposphere and the stratosphere is of strong interest. Indeed, the
842 stratospheric bromine burden is underestimated by global models that only take into account
843 long lived halons and methyl bromide. The missing source is believed to arise from bromine
844 containing very short lived substance (VSLS) (i.e: bromocarbon source gases whose lifetime
845 is less than 6 months, their degradation products as well as inorganic sources of bromine in
846 the troposphere) transported from the boundary layer to the stratosphere. Their contribution to
847 the stratospheric bromine loading ranges between 2-8 pptv (Carpenter et al., 2014). Here, we
848 find that bromine emissions from Ambrym are responsible for a mean increase of 0.3 pptv of
849 Bry in the model domain at the altitude of the plume (875 hPa), and of 0.1 pptv around 300
850 hPa in the upper troposphere (Figure 16). Local enhancements of 3 pptv are simulated in the
851 upper troposphere due to convective transport and there is also evidence of transport to the
852 stratosphere (up to 80 hPa) of Br_y from Ambrym as mentioned above. Figure 16 also presents
853 the vertical profile of daily mean Br-speciation of volcanic Br_y. We have only considered the
854 model grid boxes strongly influenced by volcanic bromine (for which the mean difference
855 between S1_HighT and S0 was higher than 0.5 pptv in Figure 21). It is clear from this figure
856 that the partitioning strongly varies with altitude. In the lower troposphere, as seen previously
857 at the local scale in Section 3.2, HBr is readily depleted by its conversion into reactive

858 bromine by the reaction of HOBr on sulfate aerosol, that produces Br_2 and/or BrCl. BrCl
859 dominates which is surprising as it is readily photolysed, and was not found to be a major
860 component of reactive bromine at the local plume-scale (section 3.2). This is most likely due
861 to very rapid halogen cycling on sulfate aerosol, whose concentration increases as more
862 volcanic SO_2 is oxidized in the downwind plume. HOBr also contributes to a significant
863 fraction of Br_y at the regional scale at 875 hPa consistent with its role of reservoir of reactive
864 bromine when the plume becomes diluted. The greater influence of photolysis reactions at
865 higher altitudes is shown in the profiles by the declining HOBr and increasing Br with altitude
866 that causes BrO also to increase. HOBr can also be washed out by precipitation. There is a
867 back-conversion of reactive bromine species (Br and BrO) into HBr at higher altitude above
868 300 hPa. It is caused by reaction of volcanic Br with HO_2. Note that the difference between
869 Br_y from S1 and from S1_HighT (not shown) is small and can reach a maximum of 3 pptv in
870 regions of Ambrym plume that reach up to 60 pptv Br_y at 875 hPa.

871 **4.2.3 Ozone**

872 Figure 17 shows the variation of ozone due to Ambrym emissions calculated as the daily
873 mean difference in percent (of S0) between the simulation S1_HighT and S0 for 12th January
874 2005. The magnitude of ozone depletion in the simulation S1_HighT is correlated with the
875 change in sulfate and in bromine due to Ambrym emissions (Figures 11 and 15). At 875 hPa,
876 it is maximal (40 %) in the concentrated plume and significant (> 10 %) in an extensive zone
877 west of the volcano strongly influenced by Ambrym emissions (Figures 11 and 15). Note that
878 during the day, the depletion can be total in the plume (not shown) as presented at plume scale
879 (Figure 8). Transport of an ozone depleted air mass by convection can also be seen at 500
880 hPa. At higher altitudes, the influence of Ambrym on ozone mixing ratios is smaller, less than
881 2%. When the whole domain is considered, Ambrym emissions are responsible for an ozone
882 depletion of 72 Gg in the S1_HighT simulation, it represents 0.2% of the ozone content in the

883 domain (32 Tg of ozone). In the S1 simulation, depletion of ozone due to Ambrym totals 69
884 Gg of ozone. It is consistent with the fact that high temperature chemistry initialization is only
885 important in approximately the first 150 kilometers from the source in our simulation as
886 shown in section 3.2.

887 **4.3 Impact of Ambrym emissions on the oxidizing power of the troposphere**

888 The oxidizing capacity of the troposphere determines the atmospheric fate of many
889 atmospheric pollutants including greenhouse gases such as methane, thus is an important
890 control on tropospheric composition and climate. Volcanic emissions are expected to impact
891 the oxidizing power of the atmosphere in several ways. First, the large amounts of SO_2
892 emitted by volcanoes react with OH, drastically reducing its concentration. Furthermore, the
893 conversion of emitted halogen halides to more reactive halogen species in volcanic plumes
894 results in chemical cycles that deplete ozone and HO_2 (and therefore OH), as well as NO_x that
895 can in turn also affect ozone and OH. In addition, these reactive halogen cycles produce
896 chlorine radicals that can also oxidize methane and non-methane hydrocarbons. Here, to
897 illustrate the impact of Ambrym during the extreme degassing event of January 2005 on the
898 oxidizing capacity of the atmosphere, we calculate change to the lifetime of a key atmospheric
899 greenhouse gas: methane. In particular, we investigate the relative contribution of the
900 different components of the volcanic emissions to the overall perturbation of methane lifetime
901 due to Ambrym degassing.

902 Methane is a key greenhouse gas with both natural and anthropogenic sources, whose main
903 loss pathway from the atmosphere is by gas-phase reaction with OH. Methane lifetime due to
904 a process (e.g., reaction with OH) is commonly defined as the total methane atmospheric
905 burden (Tg) at steady state (i.e. with unchanged burden) divided by total methane losses
906 through this process (Tg/yr) (IPCC, 2001). We have applied this definition here. However, it
907 is important to highlight that to calculate a proper methane lifetime we would have to perform

908 a simulation of about 10 years with a global model. Instead, we have calculated the
909 instantaneous perturbation of CH_4 lifetime over the model domain (averaged over a day),
910 which reflects the instantaneous perturbation of the methane sink on a regional scale. The
911 results in terms of lifetime change cannot be extrapolated to the global scale and depend also
912 strongly on the area of the model domain. Our aim here is to assess the relative contribution
913 of volcanic sulfur emissions and reactive halogen plume chemistry on the overall perturbation
914 of CH_4 lifetime.

915 We calculate that the methane lifetime due to reaction of methane with OH, τ_{CH4+OH}, is
916 about 4.65 years in our simulation when the volcanic emission from Ambrym is not included.
917 A value of 9.7 +/- 1.5 yr is derived from most recent studies based on global modeling (Naik
918 et al., 2012). The shorter methane lifetime calculated here reflects the condition in the tropics
919 for January where the OH concentration is particularly high. We find that τ_{CH4+OH} increases
920 by 0.97 % due to volcanic emissions in the simulation S1_HighT compared to the simulation
921 S0. For the simulation with volcanic SO_2 emissions alone (S1_nohal), we calculate that the
922 methane lifetime τ_{CH4+OH} increase is only about 0.37%. Therefore the increase in methane
923 lifetime, with respect to OH, due to volcanic emissions is enhanced by a factor of 2.6 when
924 reactive halogen chemistry is considered.

925 A second consideration is that the volcano plume chlorine can itself react with methane,
926 decreasing its lifetime. The methane lifetime due to reaction with Cl, τ_{CH4+Cl} is 246 years in
927 our simulation without volcanic emission from Ambrym (S0). This compares well to the
928 methane lifetime of about 200 yr derived by Allan et al. (2007). When Ambrym emissions are
929 included, τ_{CH4+Cl} decreases by 17 % to 204 years due to reaction with reactive chlorine
930 produced in Ambrym plume. Nevertheless, this reduction in methane lifetime due to Cl

931 radicals only partially counters the increase in methane lifetime caused by the decrease of OH
932 (through both volcanic plume halogen cycles and SO_2). The net volcanic impact is an overall
933 0.57 % increase in methane lifetime. Thus, the effect of chlorine radicals on the methane
934 lifetime counteracts 41% of the effect due to the OH decrease. Note that very recent
935 measurements of reactive chlorine (OClO) in Mt Etna volcanic plume (General et al., 2014;
936 Gliß et al., 2015) could help to better quantify the impact of chlorine radicals on the methane
937 lifetime.

938 **4.4 Impact of Ambrym emissions on SO_2 lifetime**

939 As already discussed in the Introduction, SO_2 undergoes atmospheric oxidation into sulfate
940 aerosols that exert climatic impacts from both direct radiative and indirect cloud albedo
941 effects (Schmidt et al., 2012). Sinks of SO_2 are dry and wet deposition, gas phase oxidation
942 and aqueous phase oxidation. The estimated lifetime of SO_2 in the troposphere by global
943 models ranges between 0.6-2.6 days (e.g., Rotstayn and Lohmann, 2002 and references
944 therein), with a lifetime with respect to gas-phase oxidation by OH of around 2 weeks (e.g.,
945 Rotstayn and Lohmann, 2002; Von Glasow 2009). However, model studies indicate a
946 lengthened lifetime for volcanic SO_2 (e.g., Chin and Jacob, 1996; Graf et al., 1997; Stevenson
947 et al., 2003; Schmidt et al., 2010). For example, a lifetime of 24-34 days was calculated for
948 the Laki 1783-4 eruption using a global model (Schmidt et al., 2010). This is due to volcanic
949 plume injection into the free troposphere (where removal rates are much lower than in the
950 boundary layer) and suppression of oxidants (OH, H_2O_2, noting limited role of ozone under
951 acid conditions) by the SO_2 chemistry. Our regional 3D model study includes a less detailed
952 SO_2-sulfate chemistry scheme (gas-phase oxidation only) but includes detailed plume reactive
953 halogen chemistry. Here, we have calculated the impact of volcanic halogen chemistry on the
954 lifetime of SO_2 due to gas phase oxidation by OH. More precisely, we calculate the lifetime of

955 SO_2 in the whole domain and of SO_2 in the plume from Ambrym (defined in our study as
956 model grids where SO_2 > 5 ppbv). For the simulation S1_nohal (that includes only SO_2
957 emissions) and for the whole domain of the simulation, we find an SO_2 lifetime of 8.8 days
958 consistent with previous work given that the simulation is for the tropics. For this S1_nohal
959 simulation and considering only the plume of Ambrym, the lifetime of SO_2 increases (11
960 days). This is consistent with the known self-limitation of SO_2 oxidation in volcanic plumes
961 as OH becomes depleted in the plume by the reaction with SO_2 itself. For the simulation
962 including volcanic halogens with high-temperature initialization, S1_HighT, the SO_2 lifetime
963 for the whole domain is 8 days and for the plume 5.5 days. This result of shorter SO_2 lifetime
964 in the plume than in the whole domain is initially surprising because of the self-limitation of
965 SO_2 oxidation as explained above. The shorter SO_2 lifetimes for S1_HighT compared to
966 S1_nohal are also again surprising because the halogen chemistry acts to further deplete OH
967 in the plume. These results are explained by the OH emissions in S1_HighT (high-
968 temperature initialization) that provides an additional rapid near-source sink for SO_2, thereby
969 contributing to the effective volcanic sulfate emission. This is confirmed by the simulation,
970 S1_nohal2 (that includes SO_2 emissions and OH emissions from HSC chemistry but no
971 halogens), in which the SO_2 lifetimes are 7.5 days for whole domain and 5.6 days for the
972 plume. This impact of high-temperature OH source on volcanic SO_2 occurs very close to
973 source (after which OH becomes depleted), leading to an unexpected shortening of the
974 calculated SO_2 lifetime, that complicates the lifetime calculation. A similar effect was not
975 seen for methane because it is not co-emitted from the volcano and OH is preferentially
976 titrated by SO_2 (and HCl).
977 Because of the complication of the lifetime calculation in S1_HighT, it is better to compare
978 the simulations with (S1) and without (S1_nohal) halogen emissions, excluding high-
979 temperature chemistry. We have shown before that simulations with and without high

temperature chemistry give very similar results in terms of Br_y and ozone at the regional scale (see sections 4.2.2 and 4.2.3). In the simulation S1, the SO_2 lifetime is 15 days in the plume and 9.4 days for the whole domain. This results is consistent with what it is expected as the lifetime of SO_2 is lengthened in the plume compared to the S1_nohal (SO_2 emission only) simulation (11 days). We conclude that including volcanic halogen chemistry increases the lifetime of SO_2 in the plume by 36 % through its impact on OH. Similarly, SO_2 lifetime is also increased by halogen chemistry for the whole domain, but by a lesser extent (9.4 days compared to 8.8 days in S1_nohal).

5. Conclusions

The CCATT-BRAMS meso-scale model was used and further developed to study the impact of Ambrym volcano emissions, Vanuatu (Southwest Pacific), on the chemical composition of the atmosphere at the local and regional scales. We focus on an episode of extreme passive degassing of Ambrym that lasted several months in early 2005, and for which SO_2 and BrO columns from airborne DOAS measurements in the plume have been reported. Model development includes the incorporation of reactive halogen chemistry and a volcano emission source specific to Ambrym. Using the nesting grid capability of CCATT-BRAMS, we simulate the Ambrym plume at high resolution (500 m × 500 m). This allows us to make a "point by point" comparison with DOAS SO_2 and BrO data, and hence test our understanding of volcanic plume chemistry at the plume level. We find that the model reproduces reasonably well the spatial distribution of SO_2 in the near downwind plume (i.e. the direction and dilution of the plume). The model captures the salient features of volcanic chemistry as reported in previous work such as HO_x and ozone depletion in the core of the plume. With the simulation initialized with high temperature chemistry at the vent (that produces: Br, Cl, HO_x and NO_x radical species), the pattern of BrO/SO_2 trend with distance downwind and across the plume simulated by the model is in good agreement with the DOAS observations. However, the

model underestimates by 60% the magnitude of observed BrO columns in the near downwind plume at 15 km. The analysis of the model results shows that BrO formation is ozone limited in the near-downwind (concentrated) plume due to the combination of a low background ozone (15 ppbv, of which 100% is depleted in the plume) and the high emissions flux from Ambrym. Further downwind in the plume at 40 km, we find a much better agreement between observed and modelled Bro columns (mean bias of 14%). This study confirms the importance of the high temperature chemistry at the vent to reproduce BrO/SO_2 variation in the near downwind plume. It also demonstrates that the (non-sulfur) radicals produced by the high temperature chemistry are mostly important for the initial rise of BrO/SO_2 at Ambrym. Further downwind from the vents (after 150 km approximately for our case), simulations with and without the high-temperature initialization exhibit rather similar chemistry. Nevertheless, the primary aerosol emission, that is crucial to enable the heterogeneous chemistry producing reactive bromine in the near downwind plume, originates from the high-temperature plume chemistry at the vent. It was kept constant in these simulations (at 1% of total sulfur) and hence its impact is not taken into account when comparing simulations with and without high temperature chemistry.

Our 3D regional model approach allows us to make the link between near downwind plume observations and regional scale observations given by satellite data. Here, we show that the model when initialized with the Ambrym SO_2 source strength estimate derived from the DOAS observations by Bani et al. (2009) and (2012) simulates SO_2 columns at the regional scale that agree within 25 % with the SO_2 columns detected by OMI. Impacts of Ambrym in Southwest Pacific region were also analyzed across the larger model grid domain. In the lower troposphere, at altitudes close to the injection height (875 hPa), Ambrym causes a substantial increase in sulfate (from 0.1 ppbv to 2.5 ppbv) and in bromine mixing ratios (from 0.1 pptv to 60 pptv). Transport of bromine species (as well as sulfate) to the upper

1030 troposphere due to convection is also predicted by the model, with convective regions
1031 confirmed by the precipitation data from the TRMM satellite as well as by trajectories from
1032 the HYSPLIT transport and dispersion model. There is also evidence in the simulations of a
1033 subsequent transport of bromine to the stratosphere from Ambrym. Thus, the halogen
1034 activation in tropospheric volcanic plumes could be one aspect of the potential impact of
1035 volcanic halogen on stratospheric ozone. In future work, longer duration simulations should
1036 be performed to fully quantify the impact of Ambrym on chemical composition of the
1037 troposphere at the regional scale. In particular, flux of bromine to upper troposphere and to
1038 the stratosphere from this extreme continuous degassing event, as well as during the typical
1039 continuous emission from Ambrym should be calculated. This will provide insight to the
1040 importance of Ambrym volcano plume to the budget and chemistry of bromine in these
1041 regions. Ozone depletion (between 5 % to 40 %) is ongoing albeit slower in the extensive
1042 region few thousands of kilometres from the volcano influenced by the dispersed plume. We
1043 find a tropospheric ozone depletion of 72 Gg, (i.e. 0.2% for a domain containing 32 Tg of
1044 ozone) in the model domain.
1045 This influence of the plume chemistry on tropospheric oxidants (depletion of HO_x and ozone
1046 by reactive halogen chemistry and depletion of OH by oxidation of SO_2) in turn affects other
1047 atmospheric species in the model. We show that methane lifetime (with respect to its reaction
1048 with OH and with Cl) in the model is increased when volcanic emissions are taken into
1049 account, confirming the potential for volcanic emissions to influence the oxidizing power of
1050 the atmosphere. Furthermore, the increase in methane lifetime, with respect to oxidation by
1051 OH, due to volcanic emissions is enhanced by a factor of 2.6 when reactive halogen chemistry
1052 is considered. Cl radicals produced in the plume counteract some of the effect (41%) of the
1053 methane lifetime lengthening due to OH depletion. This work thereby particularly highlights
1054 the impact of reactive volcanic halogen chemistry on the oxidizing capacity of the

1055 atmosphere. Here, it is found to be more important than the impact of OH depletion by
1056 volcanic SO_2. However, the reactive halogen mediated HO_x depletion and Cl radical
1057 formation exert opposing impacts on the methane lifetime. Furthermore, we calculate an
1058 increase of 36% in the SO_2 lifetime with respect to oxidation by OH when reactive halogen
1059 chemistry in the plume are included in the simulations . Thus reactive halogen chemistry
1060 exerts a significant influence on the volcanic SO_2 lifetime hence also on the production of
1061 sulfate. This needs to be taken into account in studies evaluating the impact of volcanoes on
1062 radiative forcing, especially if the injection height is high in altitude (where the sink of SO_2
1063 by OH can be the dominant oxidation pathway and thus exert a major control on SO_2 lifetime
1064 and sulfate formation, Schmidt et al., 2010). Wash-out processes were included in the model
1065 but aqueous phase of oxidation of SO_2 was not. In future this should also be included in the
1066 model, given the cloudiness of the Vanuatu region.
1067 Uncertainties in the modelled plume chemistry include aspects of the volcanic emissions, and
1068 also the rate of heterogeneous reaction of HOBr on the volcanic aerosol, which is a key driver
1069 of the reactive halogen cycling hence the plume regional impacts. This depends on the aerosol
1070 surface area and underlying chemical kinetics (for which a re-evaluation for acidic plume
1071 conditions was made by Roberts et al., 2014b). Ongoing work is aimed at improving the
1072 aerosol and HOBr reactive uptake parameterization in the model. Transects across the plume
1073 at various distances from the vents, as performed by Bani et al. (2009), appear very useful
1074 altogether with a model to test our understanding of the dynamics of volcanic plume
1075 chemistry. Nevertheless, this study emphasizes the need to measure more chemical species to
1076 constrain knowledge of the volcanic plume chemistry as also highlighted in Bobrowski et al.
1077 (2015). In particular, the coupling between BrO_x (= Br + BrO) and NO_x appears rather
1078 uncertain (Roberts et al., 2014a). Measurements of BrO and SO_2 are not sufficient to fully
1079 constrain the plume chemistry; background ozone as well as in plume ozone, HO_x, NO_x, as

well as other bromine compounds than BrO and size-resolved aerosol characterisation are needed along with a better characterisation of the plume injection height and of the plume depth (width in general being constrained by satellite and DOAS transects). To be most insightful, studies should combine the systematic downwind plume investigation with (simultaneous) detailed crater-rim measurements to constrain the volcanic gas and aerosol emission. Recent advances in satellite detection of reactive halogen species in tropospheric volcanic plumes (Hörmann et al., 2013) may also be used in future regional and global model studies of volcanic activity impacts.

Acknowledgements

This work was supported by the LABEX VOLTAIRE (VOLatils- Terre Atmosphère Interactions - Ressources et Environnement) ANR-10-LABX-100-01 (2011-20). It also benefited from the financial support of the program LEFE of the Institut National des Sciences de l'Univers of CNRS (Centre National de la Recherche Scientifique) provided to the HEVA project. The authors benefitted from the use of the cluster at the Centre de Calcul Scientifique en région Centre. We gratefully acknowledge Saulo Freitas (NOAA/ESRL/CPTEC) for his help with the CCATT-BRAMS model and Laurent Catherine (OSUC) for technical help with the cluster at Centre de Calcul Scientifique en région Centre. We thank P. Bani (IRD) and C. Oppenheimer (University of Cambridge) for providing their DOAS data, Virginie Marécal (CNRM/Météo-France) for initiating the project and Bruno Scaillet (ISTO) for providing some earlier HCl/SO_2 and HBr/SO_2 ratios. We are grateful to the NOAA Air Resources Laboratory for the provision of the HYSPLIT Transport and dispersion model (http://www.arl.noaa.gov/ready/hyslit4.html).

References

Aiuppa, A., C. Federico, A. Franco, G. Giudice, S. Gurrieri, S. Inguaggiato, M. Liuzzo, A. J. S. McGonigle, and Valenza, M.: Emission of bromine and iodine from Mount Etna volcano, Geochem. Geophys. Geosyst., 6, Q08008, doi:10.1029/2005GC000965, 2005.

Allan, W., H. Struthers, and D. C. Lowe, Methane carbon isotope effects caused by atomic chlorine in the marine boundary layer: Global model results compared with Southern Hemisphere measurements, J. Geophys. Res., 112, D04306, doi:10.1029/2006JD007369, 2007.

Allard, P., Aiuppa, A., Bani, P., Metrich, N., Bertagnini, A., Gauthier, P. J., Parelli, F., Sawyer, G. M., Shinohara, H., Bagnator, E., Mariet, C., Garebiti, E., and Pelletier, B.: Ambrym basaltic volcano (Vanuatu Arc): volatile fluxes, magma degassing rate and chamber depth, in: AGU Fall Meeting Abstracts, Vol. 1, San Francisco, United States of America, December 2009.

1127 Allard, P., Aiuppa, A., Bani, P., Métrich, N., Bertagnini, A., Gauthier, P.J., Shinohara, H.,
1128 Sawyer, G., Parello, F., Bagnato, E. and Pelletier, B.: Prodigious emission rates and magma
1129 degassing budget of major, trace and radioactive volatile species from Ambrym basaltic
1130 volcano, Vanuatu island Arc, J. Volcanol. and Geoth. R.,
1131 , doi:10.1016/j.jvolgeores.2015.10.004, in press 2015.

1132 Allibone, R., Cronin, S.J., Douglas, C.T., Oppenheimer, C., Neall, V.E., Stewart, R.B.: Dental
1133 fluorosis linked to degassing on Ambrym volcano, Vanuatu: a novel exposure, pathway.
1134 Environmental Geochemistry and Health, doi:10.1007/s10653-010-9338-2, 2010.

1135 Andres, R. J., and Kasgnoc A. D.: A time-averaged inventory of subaerial volcanic sulfur
1136 emissions, Journal of Geophysical Research: Atmospheres (1984–2012), 103, no. D19 25251-
1137 25261, 1998.

1138 Arteta, J., Marécal, V., and Riviere, E. D.: Regional modelling of tracer transport by tropical
1139 convection–Part 1: Sensitivity to convection parameterization. Atmospheric Chemistry and
1140 Physics, 9, 18, 7081-7100, 2009a.

1141 Arteta, J., Marécal, V., and Riviere, E. D. Regional modelling of tracer transport by tropical
1142 convection–Part 2: Sensitivity to model resolutions. Atmospheric Chemistry and Physics,
1143 9(18), 7101-7114, 2009b.

1144 Atkinson, R., Baulch, D. L., Cox, R. A., Crowley, J. N., Hampson, R. F., Hynes, M. E.
1145 Jenkin, M. J. Rossi, and Troe J.: Evaluated kinetic and photochemical data for atmospheric
1146 chemistry: Volume III–gas phase reactions of inorganic halogens. Atmospheric Chemistry
1147 and Physics, 7, 4, 981-1191, 2007.

1148 Bani, P., Oppenheimer C., Tsanev V. I., Carn S. A., Cronin S. J., Crimp R., Calkins J. A.,
1149 Charley D., Lardy M. and Roberts T. R.: Surge in sulphur and halogen degassing from
1150 Ambrym volcano, Vanuatu, Bulletin of Volcanology 71, 10, 1159-1168, 2009.

1151 Bani, P., Oppenheimer C., Allard P., Shinohara H., Tsanev V., Carn S., Lardy M., Garaebiti
1152 E.: First estimate of volcanic SO_2 budget for Vanuatu island arc, Journal of Volcanology and
1153 Geothermal Research, 211, 36-46, 2012.

1154 Barrie, L. A., Bottenheim, J. W., Schnell, R. C., Crutzen, P. J., and Rasmussen, R. A.: Ozone
1155 Destruction and Photochemical Reactions at Polar Sunrise in the Lower Arctic Atmosphere,
1156 Nature 334, 138 – 141,doi:10.1038/334138a0, 1988.

1157

1158 Bhartia, P. K. and Wellemeyer, C. W.: OMI TOMS-V8 Total O3 Algorithm, Algorithm
1159 Theoretical Baseline Document: OMI Ozone Products, edited by: Bhartia, P. K., Vol. II,
1160 ATBD-OMI-02,version 2.0, available at:
1161 http://eospso.gsfc.nasa.gov/sites/default/files/atbd/ATBD-OMI-02.pdf (last access: November
1162 2015).

1163 Bela, M. M., Longo K. M., Freitas S. R., Moreira D. S., Beck V., Wofsy S. C., Gerbig C.,
1164 Wiedemann K., Andreae M. O. and Artaxo P.: Ozone production and transport over the
1165 Amazon Basin during the dry-to-wet and wet-to-dry transition seasons, Atmospheric
1166 Chemistry and Physics, 15, 757-782, 2015.

1167 Bobrowski, N., G. Hönninger, B. Galle, and U. Platt: Detection of bromine monoxide in a
1168 volcanic plume, Nature, 423, 6937, 273-276, 2003.

1169 Bobrowski, N., and U. Platt: SO_2/BrO ratios studied in five volcanic plumes, Journal of
1170 Volcanology and Geothermal Research 166, 3, 147-160, 2007.

1171 Bobrowski, N., R. von Glasow, A. Aiuppa, S. Inguaggiato, I. Louban, O. W. Ibrahim, and
1172 Platt, U.: Reactive halogen chemistry in volcanic plumes, J. Geophys. Res., 112, D06311,
1173 doi:10.1029/2006JD007206, 2007.

1174 Bobrowski, N., R. Glasow, G. B. Giuffrida, D. Tedesco, A. Aiuppa, M. Yalire, S. Arellano,
1175 M. Johansson, and B. Galle.: Gas emission strength and evolution of the molar ratio of
1176 BrO/SO_2 in the plume of Nyiragongo in comparison to Etna: Journal of Geophysical
1177 Research: Atmospheres 120, 1, 277-291, 2015.

1178 Boichu, M., Oppenheimer C., Roberts T. J., Tsanev V., and Kyle P. R.: On bromine, nitrogen
1179 oxides and ozone depletion in the tropospheric plume of Erebus volcano (Antarctica).,
1180 Atmospheric Environment, 45, 23, 3856-3866, 2011.

1181 Carn, S.A., L. Clarisse and A.J. Prata, Multi-decadal satellite measurements of global
1182 volcanic degassing, *J. Volcanol. Geotherm. Res.*,
1183 http://dx.doi.org/10.1016/j.jvolgeores.2016.01.002, 2016.

1184 Carpenter L. J. and S. Reimann (Lead Authors), J.B. Burkholder, C. Clerbaux, B.D. Hall, R.
1185 Hossaini, J.C. Laube, and S.A. Yvon-Lewis, Ozone-Depleting Substances (ODSs) and Other
1186 Gases of Interest to the Montreal Protocol, Chapter 1 in Scientific Assessment of Ozone
1187 Depletion: 2014, Global Ozone Research and Monitoring Project – Report No. 55, World
1188 Meteorological Organization, Geneva, Switzerland, 2014.

1189 Carslaw, K. S., L. A. Lee, C. L. Reddington, K. J. Pringle, A. Rap, P. M. Forster, G. W.
1190 Mann, Spracklen D. V., Woodhouse M. T., Regayre L. A. and Pierce J. R.: Large contribution
1191 of natural aerosols to uncertainty in indirect forcing, Nature 503, 7474, 67-71, 2013.

1192 Chin, M., and Jacob, D. J.: Anthropogenic and natural contributions to tropospheric sulfate: A
1193 global model analysis. Journal of Geophysical Research: Atmospheres (1984–2012), 101,
1194 D13, 18691-18699, 1996.

1195 Delmelle, P.: Environmental impacts of tropospheric volcanic gas plumes. Special
1196 Publication – Geological Society of London, 213, 381-400, 2003.

1197 Diehl, T., Heil, A., Chin, M., Pan, X., Streets, D., Schultz, M., and Kinne, S.: Anthropogenic,
1198 biomass burning, and volcanic emissions of black carbon, organic carbon, and SO2 from 1980
1199 to 2010 for hindcast model experiments, Atmos. Chem. Phys. Discuss., 12, 24895-24954,
1200 doi:10.5194/acpd-12-24895-2012, 2012.

1201 Draxler, R. R. and Rolph, G. D.: HYSPLIT (HYbrid Single-Particle Lagrangian Integrated
1202 Trajectory) Model access via NOAA ARL READY Website, available at:
1203 http://ready.arl.noaa.gov/HYSPLIT.php, (last access: November 2015).

1204 Fan, S.-M. and Jacob, D. J.: Surface ozone depletion in Arctic spring sustained by bromine
1205 reactions on aerosols, Nature, 359, 522–524, 1992.

1206 Freitas, S. R., Longo, K. M., Silva Dias, M. A. F., Chatfield, R., Silva Dias, P., Artaxo, P.,
1207 Andreae, M. O., Grell, G., Rodrigues, L. F., Fazenda, A., and Panetta, J.: The Coupled
1208 Aerosol and Tracer Transport model to the Brazilian developments on the Regional
1209 Atmospheric Modeling System (CATT-BRAMS) – Part 1: Model description and evaluation,
1210 Atmos. Chem. Phys., 9, 2843-2861, doi:10.5194/acp-9-2843-2009, 2009.

1211 Freitas, S. R., Longo K. M., Alonso M. F., Pirre M., Marecal V., Grell G., Stockler R., Mello
1212 R. F., and Sánchez Gácita M.: PREP-CHEM-SRC–1.0: a preprocessor of trace gas and
1213 aerosol emission fields for regional and global atmospheric chemistry models, Geoscientific
1214 Model Development, 4, 2, 419-433, 2011.

General, S., Bobrowski, N., Pöhler D., Weber, K., Fischer, C., and Platt, U.: Airborne I-DOAS measurements at Mt. Etna: BrO and OClO evolution in the plume, J. Volcanol. Geoth. Res., 300, 175–186, doi:10.1016/j.jvolgeores.2014.05.012, 2015.

Gerlach, T. M.: Volcanic sources of tropospheric ozone-depleting trace gases, Geochem. Geophys. Geosyst., 5, *Q09007, doi:*10.1029/2004GC000747, *2004*

Gliß, J., Bobrowski, N., Vogel, L., Pöhler, D., and Platt, U.: OClO and BrO observations in the volcanic plume of Mt. Etna – implications on the chemistry of chlorine and bromine species in volcanic plumes, Atmos. Chem. Phys., 15, 5659-5681, doi:10.5194/acp-15-5659-2015, 2015.

Graf, H. F., Feichter J., and Langmann B.: Volcanic sulfur emissions: Estimates of source strength and its contribution to the global sulfate distribution, Journal of Geophysical Research: Atmospheres (1984–2012), 102, D9, 10727-10738, 1997.

Grellier, L., Marécal, V., Josse, B., Hamer, P. D., Roberts, T. J., Aiuppa, A., and Pirre, M.: Towards a representation of halogen chemistry within volcanic plumes in a chemistry transport model. Geoscientific Model Development Discussions, 7, 2, 2581-2650, 2014.

Guenther, A., Karl, T., Harley, P., Wiedinmyer, C., Palmer, P. I., and Geron, C.: Estimates of global terrestrial isoprene emissions using MEGAN (Model of Emissions of Gases and Aerosols from Nature), Atmos. Chem. Phys., 6, 3181-3210, doi:10.5194/acp-6-3181-2006, 2006.

Halmer, M. M., Schmincke H-U., and Graf H-F.: The annual volcanic gas input into the atmosphere, in particular into the stratosphere: a global data set for the past 100 years, Journal of Volcanology and Geothermal Research, 115, 3, 511-528, 2002.

1237 Hebestreit, K.; Stutz, J.; Rosen, D.; Matveiv, V.; Peleg, M.; Luria M.; Platt, U.: DOAS
1238 measurements of tropospheric bromine oxide in mid-latitudes, Science, 283, 55−57, 1999.

1239 Hörmann, C., Sihler H., Bobrowski N., Beirle S., Penning de Vries M., Platt U., and Wagner
1240 T.: Systematic investigation of bromine monoxide in volcanic plumes from space by using the
1241 GOME-2 instrument., Atmos. Chem. Phys, 13, 4749-4781, 2013.

1242 Huffman, G.J., R.F. Adler, D.T. Bolvin, G. Gu, E.J. Nelkin, K.P. Bowman, Y. Hong, E.F.
1243 Stocker and Wolff, D. B.: The TRMM Multi-satellite Precipitation Analysis: Quasi-Global,
1244 Multi-Year, Combined-Sensor Precipitation Estimates at Fine Scale. J. Hydrometeor., 8(1),
1245 38-55, 2007.

1246 Josse, B., Simon P., and Peuch V-H.: Radon global simulations with the multiscale chemistry
1247 and transport model MOCAGE, Tellus B, 56, 4, 339-356, 2004.

1248 Kelly, P. J., Kern C., Roberts T. J., Lopez T., Werner C., Aiuppa A.: Rapid chemical
1249 evolution of tropospheric volcanic emissions from Redoubt Volcano, Alaska, based on
1250 observations of ozone and halogen-containing gases, Journal of Volcanology and Geothermal
1251 Research, 259, 317-333, 2013.

1252 Kern, C., Sihler H., Vogel L., Rivera C., Herrera M. and Platt U.: Halogen oxide
1253 measurements at Masaya Volcano, Nicaragua using active long path differential optical
1254 absorption spectroscopy, Bulletin of volcanology, 71, 6, 659-670, 2009.

1255 Kern, C., T. Deutschmann, L. Vogel, M. Wöhrbach, T. Wagner, and U. Platt, Radiative
1256 transfer corrections for accurate spectroscopic measurements of volcanic gas emissions, Bull.
1257 Volcanol., 72, 233–247,doi:10.1007/s00445-009-0313-7, 2010.

1258 Kern, C., T. Deutschmann, C. Werner, A. J. Sutton, T. Elias, and P. J. Kelly, Improving the
1259 accuracy of SO2 column densities and emission rates obtained from upward-looking UV-

spectroscopic measurements of volcanic plumes by taking realistic radiative transfer into account, J. Geophys. Res.,117, D20302, doi:10.1029/2012JD017936, 2012.

Kurosu, T. P., Chance K., and Sioris C. E.: Preliminary results for HCHO and BrO from the EOS-aura ozone monitoring instrument, In Fourth International Asia-Pacific Environmental Remote Sensing Symposium 2004: Remote Sensing of the Atmosphere, Ocean, Environment, and Space, pp. 116-123. International Society for Optics and Photonics, 2004.

Lee, C., Kim Y.J., Tanimoto H., Bobrowski N., Platt U., Mori T., Yamamoto K., Hong *C.S.:* High ClO and ozone depletion observed in the plume of Sakurajima volcano, Japan, Geophys. Res. Lett., 32, L21809, doi:10.1029/2005GL023785, 2005.

Lefèvre, J., Menkes, C., Bani, P., Marchesiello, P., Curci, G., Grell, G., and Frouin, R. : Distribution of sulfur aerosol precursors in the SPCZ released by continuous volcanic degassing at Ambrym, Vanuatu, *J. Volcanol. Geoth. Res.*, doi:10.1016/j.jvolgeores.2015.07.018, in press 2015.

Li, C., J. Joiner, N. A. Krotkov, and Bhartia P. K., A fast and sensitive new satellite SO2 retrieval algorithm based on principal component analysis:Application to the ozone monitoring instrument, Geophys. Res. Lett., 40, 6314–6318, doi:10.1002/2013GL058134, 2013.

Livesey, N.J., et al., 2011. Earth Observing System (EOS) Aura Microwave Limb Sounder (MLS) Version 3.3 and 3.4 Level 2 Data Quality and Description Document. Tech. Rep. JPL D-33509. NASA Jet Propulsion Laboratory, California Institute of Technology, Pasadena, California (91109-8099, available at: http://mls.jpl.nasa.gov/data/datadocs.php).

1281 Logan, J. A., An analysis of ozonesonde data for the troposphere: Recommendations for
1282 testing 3-D models and development of a gridded climatology for tropospheric ozone, J.
1283 Geophys. Res., 104(D13), 16,115–16,149, doi:10.1029/1998JD100096,1999.

1284 Longo, K. M., Freitas, S. R., Pirre, M., Marécal, V., Rodrigues, L. F., Panetta, J., Alonso, M.
1285 F., Rosário, N. E., Moreira, D. S., Gácita, M. S., Arteta, J., Fonseca, R., Stockler, R.,
1286 Katsurayama, D. M., Fazenda, A., and Bela, M.: The Chemistry CATT-BRAMS model
1287 (CCATT-BRAMS 4.5): a regional atmospheric model system for integrated air quality and
1288 weather forecasting and research, Geosci. Model Dev., 6, 1389-1405, doi:10.5194/gmd-6-
1289 1389-2013, 2013.

1290 Marécal, V., Pirre M., Krysztofiak G., Hamer P. D., and Josse B.: what do we learn about
1291 bromoform transport and chemistry in deep convection from fine scale modelling?,
1292 Atmospheric Chemistry and Physics, 12, 14, 6073-6093, 2012.

1293 Martin, R. S., Mather, *T. .A. and* Pyle, D. M. *:* High-temperature mixtures of magmatic and
1294 atmospheric gases, Geochem. Geophys. Geosyst., 7, *Q04006, doi:*10.1029/2005GC001186,
1295 *2006*.

1296 Martin, R. S., Roberts T. J., Mather T. A., and Pyle D. M.: The implications of H_2S and H_2
1297 kinetic stability in high-T mixtures of magmatic and atmospheric gases for the production of
1298 oxidized trace species (eg, BrO and NOx), Chemical Geology, 263, 1, 143-159, 2009.

1299 Martin, R. S., Ilyinskaya E., and Oppenheimer C.: The enigma of reactive nitrogen in
1300 volcanic emissions, Geochimica et Cosmochimica Acta, 95, 93-105, 2012.

1301 Mather, T. A., A. G. Allen, C. Oppenheimer, D. M. Pyle, and A. J. S. McGonigle: Size-
1302 resolved characterisation of soluble ions in the particles in the tropospheric plume of Masaya

1303 volcano, Nicaragua: Origins and plume processing, Journal of Atmospheric Chemistry 46, 3,
1304 207-237, 2003.

1305 Mather T.A, Pyle D.M, Allen A.G: Volcanic source for fixed nitrogen in the early Earth's
1306 atmosphere. Geology. 32, 905–908, doi:10.1130/G20679.1, 2004.

1307 Mosca, S.G.; Graziani, W.; Klug, R.; Bellasio; Bianconi R., "A statistical methodology for the
1308 evaluation of long-range dispersion models: An application to the ETEX exercise,", Atmos.
1309 Environ., 32, 4302–4324, 1998.

1310 Myhre, G., D. Shindell, F.-M. Bréon, W. Collins, J. Fuglestvedt, J. Huang, D. Koch, J.-F.
1311 Lamarque, D. Lee, B. Mendoza, T. Nakajima, A. Robock, G. Stephens, T. Takemura and H.
1312 Zhang, 2013: Anthropogenic and Natural Radiative Forc¬ing. In: Climate Change 2013: The
1313 Physical Science Basis. Contribution of Working Group I to the Fifth Assessment Report of
1314 the Intergovernmental Panel on Climate Change [Stocker, T.F., D. Qin, G.-K. Plattner, M.
1315 Tignor, S.K. Allen, J. Boschung, A. Nauels, Y. Xia, V. Bex and P.M. Midgley (eds.)].
1316 Cambridge University Press, Cambridge, United Kingdom and New York, NY, USA.

1317 Naik, V., Voulgarakis, A., Fiore, A. M., Horowitz, L. W., Lamarque, J.-F., Lin, M., Prather,
1318 M. J., Young, P. J., Bergmann, D., Cameron-Smith, P. J., Cionni, I., Collins, W. J., Dalsøren,
1319 S. B., Doherty, R., Eyring, V., Faluvegi, G., Folberth, G. A., Josse, B., Lee, Y. H.,
1320 MacKenzie, I. A., Nagashima, T., van Noije, T. P. C., Plummer, D. A., Righi, M., Rumbold,
1321 S. T., Skeie, R., Shindell, D. T., Stevenson, D. S., Strode, S., Sudo, K., Szopa, S., and Zeng,
1322 G.: Preindustrial to present-day changes in tropospheric hydroxyl radical and methane
1323 lifetime from the Atmospheric Chemistry and Climate Model Intercomparison Project
1324 (ACCMIP), Atmos. Chem. Phys., 13, 5277-5298, doi:10.5194/acp-13-5277-2013, 2013.

1325 Oppenheimer, C., Tsanev V. I., Braban C.F., Cox R. A., Adams J. W., Aiuppa A., Bobrowski
1326 N., Delmelle P., Barclay J., McGonigle A.J. S.: BrO formation in volcanic plumes,
1327 Geochimica et Cosmochimica Acta, 70, 12, 2935-2941, 2006.

1328 Oppenheimer, C., Kyle, P., Eisele, F., Crawford, J., Huey, G., Tanner, D., Kim, S., Maudlin,
1329 L., Blake, D., Beyersdorf, A., Bubr, M., and Davis, D.: Atmospheric chemistry of an
1330 Antarctic volcanic plume, J. Geophys. Res., 115, D04303, doi:10.1029/2009JD011910, 2010.

1331 Popp C., McCormick B., Suleiman R., Chance K., Andrews B., Cottrell E.: Analysis of
1332 volcanic bromine monoxide emissions in the southwestern Pacific region in 2005 based on
1333 satellite observations from OMI, Geophysical Research Abstracts Vol. 17, EGU2015-9837,
1334 2015.

1335 Putirka, K. D.: Thermometers and barometers for volcanic systems. In: Putirka, K. D. &
1336 Tepley, F. (Eds.), Minerals, Inclusions and Volcanic Processes, Reviews in Mineralogy and
1337 Geochemistry 69, 61–120, 2008.

1338 Prata, A.J., Carn, S.A., Stohl, A., Kerkmann, J., Long range transport and fate of a
1339 stratospheric volcanic cloud from Soufrière Hills volcano, Montserrat. Atmos. Chem.
1340 Phys. 7, 5093–5103, 2007.

1341 Pyle, D. M., and Mather T. A.: Halogens in igneous processes and their fluxes to the
1342 atmosphere and oceans from volcanic activity: a review." Chemical Geology, 263, 1, 110-
1343 121, 2009.

1344 Remer, L.A., Kaufman, Y.J., Tanre, D., Mattoo, S., Chu, D.A., Martins, J.V., Li, R.R.,
1345 Ichoku, C., Levy, R.C., Kleidman, R.G., Eck, T.F., Vermote, E., Holben, B.N., The MODIS
1346 aerosol algorithm, products, and validation. J. Atmos. Sci. 62 (4), 947–973, 2005.

1347 Remer, L.A., Kleidman R. G., Levey R.C., Kaufmann Y.J., Tanré D., Mattoo S., Martins J.V.,
1348 Ichoku C., Koren I., Yu H., Holben B.N., Global aerosol climatology from the MODIS
1349 satellite sensors, J. Geophys. Res., 113, D14S07, doi:10.1029/2007JD009661, 2008.

1350 Roberts, T. J., Braban C. F., Martin R. S., Oppenheimer C., Adams J. W., Cox R. A., Jones R.
1351 L., and Griffiths P. T.: Modelling reactive halogen formation and ozone depletion in volcanic
1352 plumes, Chemical Geology, 263, 1, 151-163, 2009.

1353 Roberts, T. J., Martin, R. S. and Jourdain L.: Reactive bromine chemistry in Mount Etna's
1354 volcanic plume: the influence of total Br, high-temperature processing, aerosol loading and
1355 plume–air mixing, Atmospheric Chemistry and Physics, 14, 20, 11201-11219, 2014a.

1356 Roberts, T. J., Jourdain L., Griffiths P. T., and Pirre M., Re-evaluating the reactive uptake of
1357 HOBr in the troposphere with implications for the marine boundary layer and volcanic
1358 plumes, Atmospheric Chemistry and Physics, 14, 20, 11185-11199, 2014b.

1359 Roberts T. J., Vignelles D., Liuzzo M., Giudice G., Aiuppa A., Chartier M., Coute B., Lurton
1360 T., Berthet G., Renard J.-B., Advances in in-situ real-time monitoring of volcanic emissions:
1361 HCl, and size-resolved aerosol at Mt Etna (passive degassing), submitted to Geochimica et
1362 Cosmochimica Acta, 2015.

1363 Robin, C., Eissen, J.-P. and Monzier, M.: Giant tuff cone and 12-kin-wide associated caldera
1364 at Ambrym Volcano (Vanuatu, New Hebrides Arc). J. Volcanol. Geotherm. Res., 55: 225-
1365 238, 1993.

1366 Roine A.: HSC Chemistry 6.1, Tech. rep. Outotec Research Oy, Pori, Finland, 2007.

1367 Rosário, N. E., Longo K. M., Freitas S. R., Yamasoe M. A., and Fonseca R. M.: Modeling the
1368 South American regional smoke plume: aerosol optical depth variability and surface
1369 shortwave flux perturbation, Atmos. Chem. Phys, 13, 2923-2938, 2013.

1370 Rotstayn, L. D., and U. Lohmann, Simulation of the tropospheric sulfur cycle in a global
1371 model with a physically based cloud scheme, J. Geophys. Res., 107(D21), 4592,
1372 doi:10.1029/2002JD002128, 2002.

1373 Saiz-Lopez, A., J. M. C. Plane, and J. A. Shillito : Bromine oxide in the mid-latitude

1374 marine boundary layer, Geophys. Res. Lett., 31, L03111, doi:10.1029/2003GL018956, 2004.

1375 Sander, R.: Compilation of Henry's Law Constants for Inorganic and Organic Species of
1376 Potential Importance in Environmental Chemistry, available at: http://www.henrys-
1377 law.org/henry-3.0.pdf (last access: November 2015), 1999.

1378 Sander, S. P., Friedl, R. R., Golden, D. M., Kurylo, M. J., Moortgat, G. K., Keller-Rudek, H.,
1379 Wine, P. H., Ravishankara, A. R., Kolb, C. E., Molina, M. J., Finlayson-Pitts, B. J., Huie, R.
1380 E., and Orkin, V. L.: Chemical Kinetics and Photochemical Data for Use in Atmospheric
1381 Studies, Evaluation Number 15, JPL Publication 06-2, Jet Propulsion Laboratory, Pasadena,
1382 CA, available at http://jpldataeval.jpl.nasa.gov/pdf/JPL_15_AllInOne.pdf (last access:
1383 November 2015), 2006.

1384 Schmidt, A., Carslaw K. S., Mann G. W., Wilson M., Breider T. J., Pickering S. J., and
1385 Thordarson T: The impact of the 1783–1784 AD Laki eruption on global aerosol formation
1386 processes and cloud condensation nuclei. Atmospheric Chemistry and Physics 10, 13, 6025-
1387 6041, 2010.

1388 Schmidt, A., Carslaw K. S., Mann G. W., Rap A., Pringle K. J., Spracklen D. V., Wilson M.,
1389 and Forster P. M.: Importance of tropospheric volcanic aerosol for indirect radiative forcing
1390 of climate, Atmospheric Chemistry and Physics, 12, 16, 7321-7339, 2012.

1391 Simpson, W. R., Brown S. S., Saiz-Lopez A., Thornton J. A., and von Glasow R..:
1392 Tropospheric Halogen Chemistry: Sources, Cycling, and Impacts, Chemical reviews, 2015.

1393 Schultz, M., Backman, L., Balkanski, Y., Bjoerndalsaeter, S., Brand, R., Burrows, J.,
1394 Dalsoeren, S., de Vasconcelos, M., Grodtmann, B., Hauglustaine, D., Heil, A., Hoelzemann,
1395 J., Isaksen, I., Kaurola, J., Knorr, W., Ladstaetter-Weienmayer, A., Mota, B., Oom, D.,
1396 Pacyna, J., Panasiuk, D., Pereira, J., Pulles, T., Pyle, J., Rast, S., Richter, A., Savage, N.,
1397 Schnadt, C., Schulz, M., Spessa, A., Staehelin, J., Sundet, J., Szopa, S., Thonicke, K., van het
1398 Bolscher, M., van Noije, T., van Velthoven, P., Vik, A., and Wittrock, F.: REanalysis of the
1399 TROpospheric chemical composition over the past 40 years (RETRO). A long-term global
1400 modeling study of tropospheric chemistry. Final Report, Tech. rep., Max Planck Institute for
1401 Meteorology, Hamburg, Germany, 2007.

1402 Schumann, U., Weinzierl, B., Reitebuch, O., Schlager, H., Minikin, A., Forster, C., Baumann,
1403 R., Sailer, T., Graf, K., Mannstein, H., Voigt, C., Rahm, S., Simmet, R., Scheibe, M.,
1404 Lichtenstern, M., Stock, P., Rüba, H., Schäuble, D., Tafferner, A., Rautenhaus, M., Gerz, T.,
1405 Ziereis, H., Krautstrunk, M., Mallaun, C., Gayet, J.-F., Lieke, K., Kandler, K., Ebert, M.,
1406 Weinbruch, S., Stohl, A., Gasteiger, J., Groß, S., Freudenthaler, V., Wiegner, M., Ansmann,
1407 A., Tesche, M., Olafsson, H., and Sturm, K.: Airborne observations of the Eyjafjalla volcano
1408 ash cloud over Europe during air space closure in April and May 2010, Atmos. Chem. Phys.,
1409 11, 2245-2279, doi:10.5194/acp-11-2245-2011, 2011.

1410 Seinfeld, J. H. and Pandis, A. N.: Properties of the atmospheric aerosol, in: Atmospheric
1411 Chemistry and Physics – from Air Pollution to Climate Change, Chapter 8, John Wiley and
1412 Sons, New Jersey, United States of America, 350–394, 2006.

1413 Siebert, L., Simkin, T., and Kimberly, P.: Volcanoes of the World, 3rd ed. Berkeley:
1414 University of California Press, United States of America, 568 p, 2010.

1415 Sheehan, F. and Barclay, J.: Staged storage and magma recycling at Ambrym volcano,
1416 Vanuatu, J. Volcanol. Geoth. Res., doi:10.1016/j.jvolgeores.2016.02.024, in press 2016.

1417 Simpson, W. R., Brown, S. S., Saiz-Lopez, A., Thornton, J. A., and von Glasow, R.:
1418 Tropospheric halogen chemistry: sources, cycling, and impacts, Chem. Rev., 115 (10), pp
1419 4035–4062, doi**:** 10.1021/cr5006638, 2015.

1420 Stevenson, D. S., Johnson C. E., Collins W. J., and Derwent R. G.: The tropospheric sulphur
1421 cycle and the role of volcanic SO_2, Geological Society, London, Special Publications 213, 1,
1422 295-305, 2003.

1423 Stockwell, W. R., Kirchner F., Kuhn M. and Seefeld S.: A new mechanism for regional
1424 atmospheric chemistry modeling, Journal of Geophysical Research: Atmospheres (1984–
1425 2012), 102, D22, 25847-25879, 1997.

1426 Surl, L., Donohoue D., Aiuppa A., Bobrowski N., and von Glasow R.: Quantification of the
1427 depletion of ozone in the plume of Mount Etna, Atmospheric Chemistry and Physics 15, 5
1428 2613-2628, 2015.

1429 Tabazadeh, A., Toon O. B., Clegg S. L., Hamill P.: A new parameterization of H2SO4/H2O
1430 aerosol composition: Atmospheric implications, Geophysical Research Letters, 24, 15, 1931-
1431 1934, 1997.

1432 Theys, N., M. Van Roozendael, B. Dils, F. Hendrick, N. Hao, and De Mazière M. : First
1433 satellite detection of volcanic bromine monoxide emission after the Kasatochi eruption,
1434 Geophys. Res. Lett., 36, L03809, doi:10.1029/2008GL036552, 2009.

1435 Theys, N., De Smedt, I., Van Roozendael, M., Froidevaux, L., Clarisse, L., Hendrick, F.,
1436 First satellite detection of volcanic OClO after the eruption of Puyehue-Cordón Caulle.

1437 Geophys. Res. Lett. 41, 667–672. http://dx.doi.org/10.1002/2013GL058416, 2014.

1438 Tie, X., S. Madronich, S. Walters, R. Zhang, P. Rasch, and Collins W., Effect of clouds on
1439 photolysis and oxidants in the troposphere, J. Geophys. Res., 108, 4642,
1440 doi:10.1029/2003JD003659, 2003.

1441 Vance, A., A. J. S. McGonigle, A. Aiuppa, J. L. Stith, K. Turnbull, and von Glasow R.,
1442 Ozone depletion in tropospheric volcanic plumes, Geophys. Res. Lett., 37, L22802,
1443 doi:10.1029/2010GL044997, 2010.

1444 van der Werf, G. R., Randerson J. T., Giglio L., Collatz G. J., Kasibhatla P. S. and Arellano
1445 Jr, A. F.: Interannual variability in global biomass burning emissions from 1997 to 2004,
1446 Atmospheric Chemistry and Physics, 6, 11, 3423-3441, 2006.

1447 Voigt, C., P. Jessberger, T. Jurkat, S. Kaufmann, R. Baumann, H. Schlager, N. Bobrowski, G.
1448 Giuffrida, and G. Salerno: Evolution of CO2, SO2, HCl, and HNO3 in the volcanic plumes
1449 from Etna, Geophysical Research Letters, 41, 6, 2196-2203, 2014.

1450 von Glasow, R., Bobrowski N., and Kern C.: The effects of volcanic eruptions on atmospheric
1451 chemistry, Chemical Geology, 263, 1, 131-142, 2009.

1452 von Glasow, R.: Atmospheric chemistry in volcanic plumes, Proceedings of the National
1453 Academy of Sciences, 107, 15, 6594-6599, 2010.

1454 Walko, R. L., Band L. E., Baron J., Kittel T. G. F., Lammers R., Lee T. J., Ojima D., Pielke
1455 Sr R. A., Tayloer C., Tague C., Tremback C. J., Vidale P.L: Coupled atmosphere-biophysics-
1456 hydrology models for environmental modeling. Journal of applied meteorology, 39, 6, 931-
1457 944, 2000.

1458 Wang T. X., Kelley M. D., Cooper J. N., Beckwith R. C., and Margerum D. W.: Equilibrium,
1459 kinetic, and UV-spectral characteristics of aqueous bromine chloride, bromine, and chlorine
1460 species, Inorganic Chemistry, 33, 25, 5872-5878, 1994.

1461

Tables:

Reaction	Reactive uptake coefficient
$HOBr + H^+_{(aq)} + Br^-_{(aq)} \rightarrow Br_{2(aq \rightarrow g)} + H_2O$	$0.2 \times \frac{[Br_{2(aq)}]}{[Br_{2(aq)}] + [BrCl_{(aq)}]}$
$HOBr + H^+_{(aq)} + Cl^-_{(aq)} \rightarrow BrCl_{(aq \rightarrow g)} + H_2O$	$0.2 \times \frac{[BrCl_{(aq)}]}{[Br_{2(aq)}] + [BrCl_{(aq)}]}$
$BrONO_2 + H_2O \rightarrow HOBr_{(aq \rightarrow g)} + HNO_3$	0.8

Table 1: Heterogeneous reactions in the model and their associated reactive uptake coefficients on sulfate aerosol. See section 2.3.1 for description of the calculation of the ratio $\frac{[BrCl_{(aq)}]}{[Br_{2(aq)}]}$.

Volcano	Reported activity	Emission (kt/day)	Source
Gaua	None	0,070 kt/day	AEROCOM database (a)
Aoba (Ambae)	None	0.070 kt/day	AEROCOM database (b)
Ambrym	Extreme passive degassing	18.835 kt/day	Bani et al. (2012) (c)
Lopevi	Not clear	0.070 kt/day	Bani et al. (2012) (d)
Epi	None	0.070 kt/day	AEROCOM database (e)
Yasur	Eruption	0.968 kt/day	Bani et al. (2012) (f)

Table 2: SO_2 emission rates in January 2005 from the principal active Vanuatu's volcanoes (Gaua, Aoba, Lopevi, Epi, Ambrym, Yasur) as prescribed in the simulations. Details for each volcano are given in the following:

a) In Bani et al. (2012), only information during a phase of eruptive activity. We prescribed the post eruptive degassing rate (for the volcanoes that had an eruption since 1900) of 0.070 kt/day assigned for this volcano in the AEROCOM database.

b) Before eruption of nov. 2005, no significant passive degassing. We prescribed the post eruptive degassing rate of 0.070 kt/day assigned in the AEROCOM database.

c) Mean of 5 transverses of 12 January 2005 in Bani et al. (2012). Note that, in the fourth grid, the two Marum and Benbow cones do not lie in the same gridbox. As a result, we prescribed 60% of the emission in the model gridbox containing Marum and 40% in the gridbox containing Benbow as found in Bani et al. (2009). Note, that in the AEROCOM database, the value is 0.0807kt/day.

d) Lopevi is a volcano with frequent degassing. From Bani et al. (2006), vapor was observed covering the crater but it was difficult to conclude on its volcanic activy. Local observers in Vanuatu indicated ongoing eruptive activity at Lopevi starting at the end of January 2005 and continuing on February (GPV). Mean of 3 traverses of passive degassing of 24/02/2006 was 0.156 kt/day. As a result, we kept the value of AEROCOM database of 0.070 kt/day.

e) No information. Post eruptive degassing rate of 0.070 kt/day is assigned in AEROCOM database.

f) Value of 10/01/05 of Bani et al. (2012). In AEROCOM database, it is 0.900 kt/day

Gas	Mass mixing ratio in HSC input
H_2O	9.29 E-01
N_2	1.56E-02
CO_2	3.80E-02
SO_2	1.05E-02
HCl	1.84E-03
O_2	4.20E-03
Ar	2.00E-04
HBr	7.23E-06
HF	7.53E-04

Table 3: Composition inputs to the HSC Chemistry model assuming plume-air mixture of 98:2 magmatic:atmospheric gases, with temperatures 1125 ˚C and 20 ˚C, resulting in mixed temperature of 1103 ˚C. Resulting output of the HSC Chemistry simulations were converted to ratios relative to sulfur and used to initialize the S1_HighT model simulation (second row of Table 4). The HSC Chemistry model is presented in section 2.3.3

Simulations	HCl/SO_2	HBr/SO_2	H_2SO_4/SO_2	Cl/SO_2	Br/SO_2	OH/SO_2	NO/SO_2
S1	0.1	8.75e-04	1.55e-02	0	0	0	0
S1_HighT	0.1	6.87e-04	1.55e-02	1.33e-04	1.89e-04	7.04e-04	7.45e-04
S1_HighT_noNOx	0.1	6.87e-04	1.55e-02	1.33e-04	1.89e-04	7.04e-04	0
S1_no_hal Ambrym only	0	0	0	0	0	0	0
S1_no_hal2 Ambrym only	0	0	0	0	0	7.04e-04	0
S0 Ambrym only	0	0	0	0	0	0	0

Table 4: Emissions of HCl, HBr, sulfate and radicals (Cl, Br, OH, NO) expressed in terms of mass ratios relative to SO_2 emissions for all the volcanoes within the domain study and for the different simulations (see section 2.3.3 for the details on the ratios derivation and section 2.3.4 for details on the simulations). Note that for S1_no_hal, S1_no_hal2 and S0 simulations, the ratios indicated here are only for the emissions of the Ambrym volcano.

These simulations have the same emissions than S1_HighT for the other volcanoes within the domain study. Note also that all the simulations, except S0, have an SO_2 emission for Ambrym of 18.8 kt/day S0 does not include any volcanic emissions from Ambrym.

	Mean SO_2	Mean BrO	r_{SO2}	r_{BrO}	$RMSE_{SO2}$	$RMSE_{BrO}$
DOAS	2.29 e18	5.84 e14				
S1	2.27 e18	1.14 e14	0.62	-0.21	1.09e18	5.97e14
S1_HighT	2.25e18	3.42e14	0.61	0.59	1.10e18	3.90e14

Table 5: Statistical comparison between the DOAS SO_2 and BrO columns from the 5 traverses of the Ambrym plume on 12 th January 2005 and the corresponding simulated values (for S1 and S1_HighT). Correlation coefficients (r), root mean square error (RMSE in molecule. cm^{-2})) are given as well as mean values (molecule. cm^{-2}) of observed and simulated data. Note that we did not include here the data for which we did not have GPS data (dashed lines of Figures 3 and 4).

1570

1571

1572

1573

1574

1575

1576

1577

1578

1579

1580

1581

Figure captions:

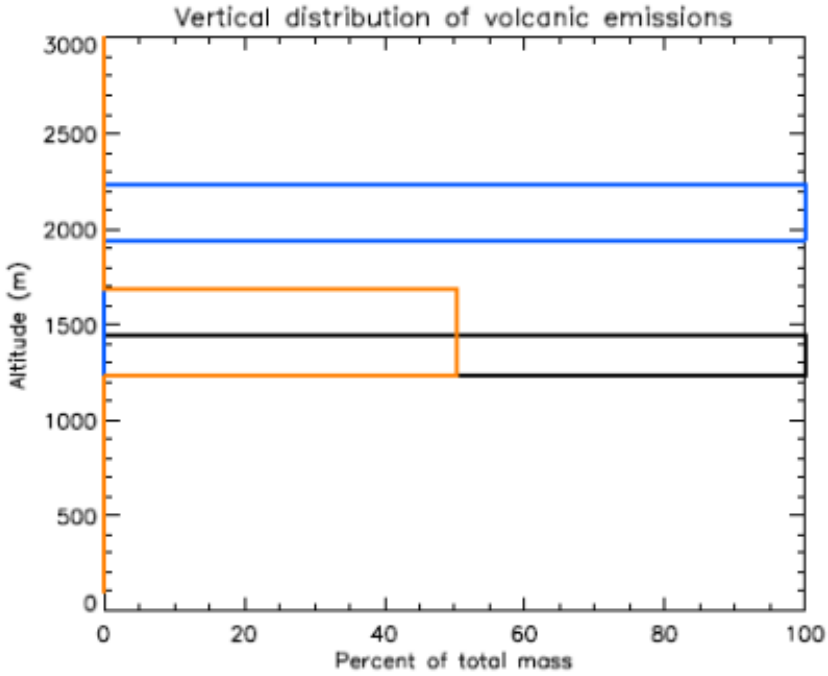

Figure 1: Vertical distribution of volcanic emissions from Ambrym as prescribed in the model for the all the simulations (black line) except for the sensitivity simulations S1_HighT_alt (blue line), S1_HighT_width (orange line). See section 2.3.4 for details on simulations.

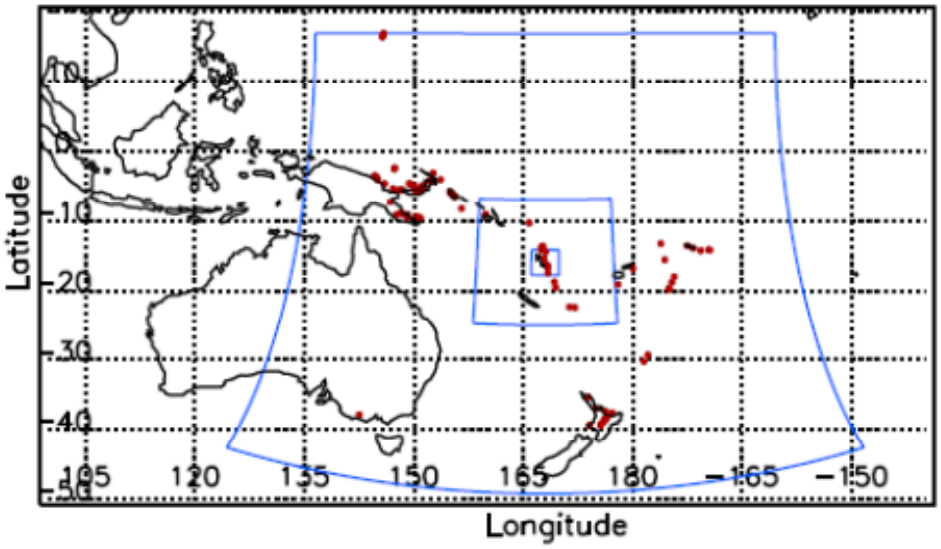

1597

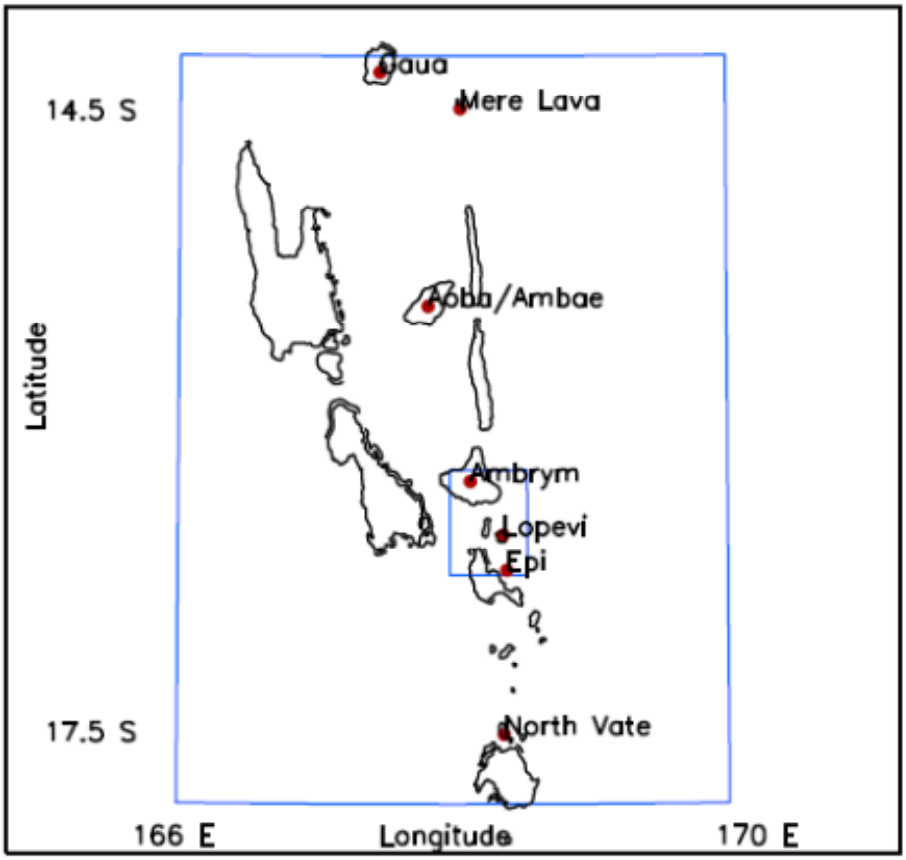

1598

1599 **Figure 2:** a) Top: Position of the nested model grids (blue lines) and of the volcanoes (red
1600 filled circles) taken into account in the simulations. For clarity, only the 3 largest model grids
1601 are shown. b) Bottom: Zoom on the two smallest model grids (blue lines) and on the

volcanoes (red filled circles) taken into account in the simulations. Resolution of each grid is given in section 2.3.4.

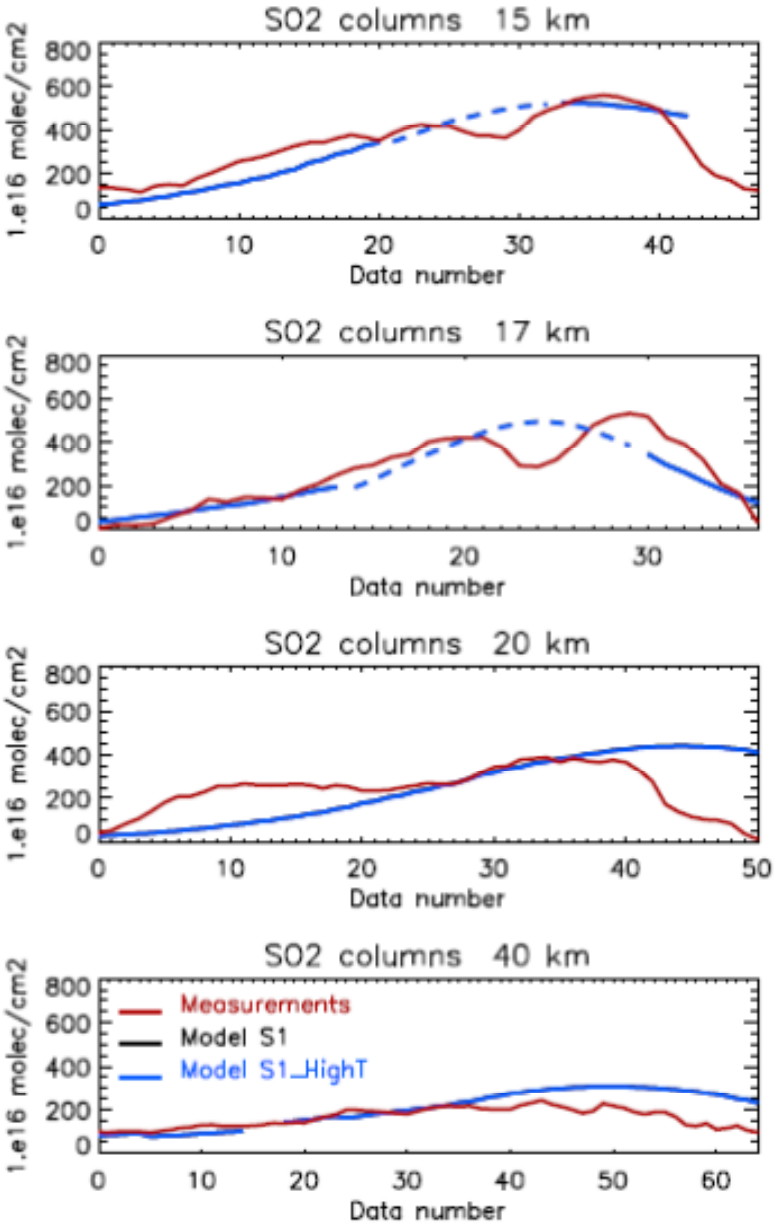

Figure 3: Comparison between SO_2 columns observed by Bani et al. (2009) (red line) and simulated by the model for S1 (black line), S1_HighT (blue line). Each panel represents a traverse of the Ambrym plume in the cross-wind direction on the 12 th January 2005 between 05:00 UT and 06:00 UT, at a range of distances downwind. The traverse at 21 km from the source is not shown here but is included in Table 5. The x-axis shows the datapoint number in the transect across the plume (Bani et al., 2009). The direction of each transect across the plume has a east-west component. Here, each transect is shown with the datapoints from

1634 west to east (left to right). Note that model results are for the same position and time as the
1635 measurements and for the finest grid (0.5 km x0.5 km) except when GPS data (longitude and
1636 latitude) were not available. In this case, model results (dashed lines) were interpolated
1637 between the last and the next positions for which we had GPS data. Note that black and blue
1638 lines are on top of each other (superimposed). Reported error from DOAS measurements (1 σ)
1639 is 2.45×10^{16} molec./cm^2
1640
1641
1642
1643
1644
1645
1646
1647
1648
1649
1650
1651
1652
1653
1654
1655
1656
1657

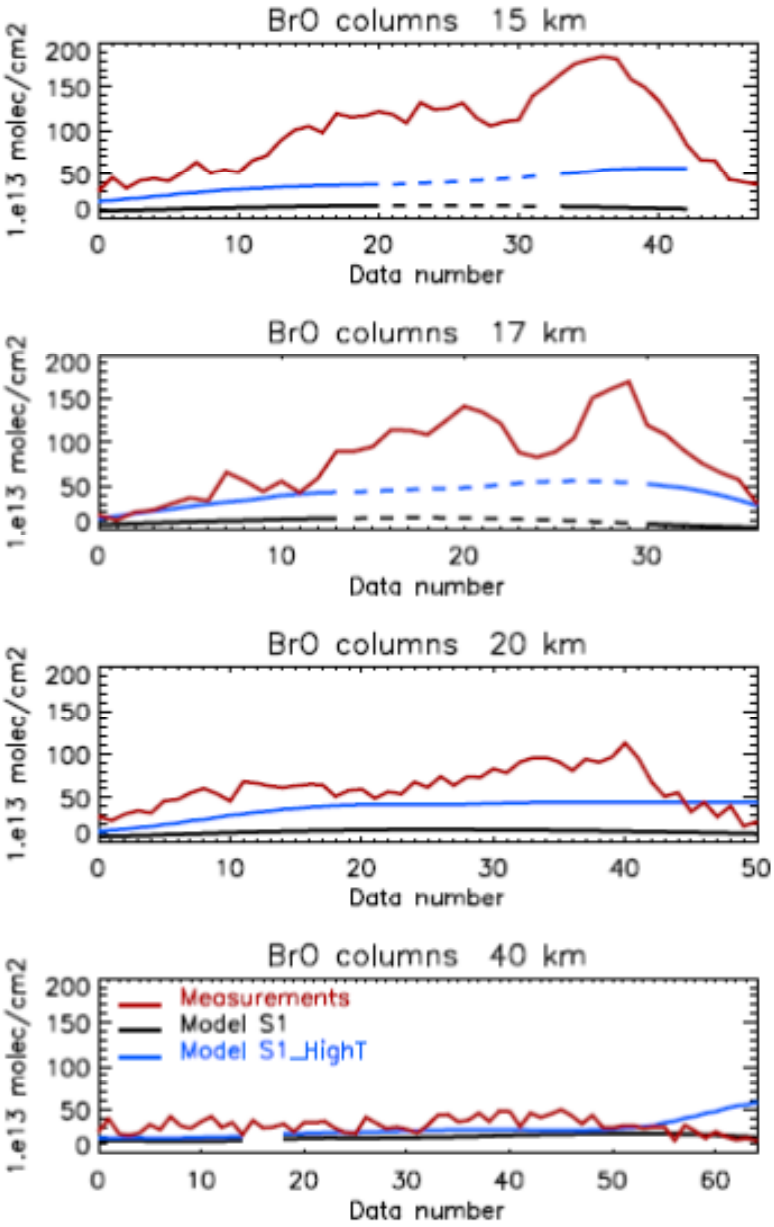

Figure 4: Comparison between BrO columns observed by Bani et al. (2009) (red line) and simulated by the model for S1 (black line), S1_HighT (blue line). See Figure 3 for details on the method of comparison. Reported error (1 σ) is 1.22×10^{14} molec./cm^2.

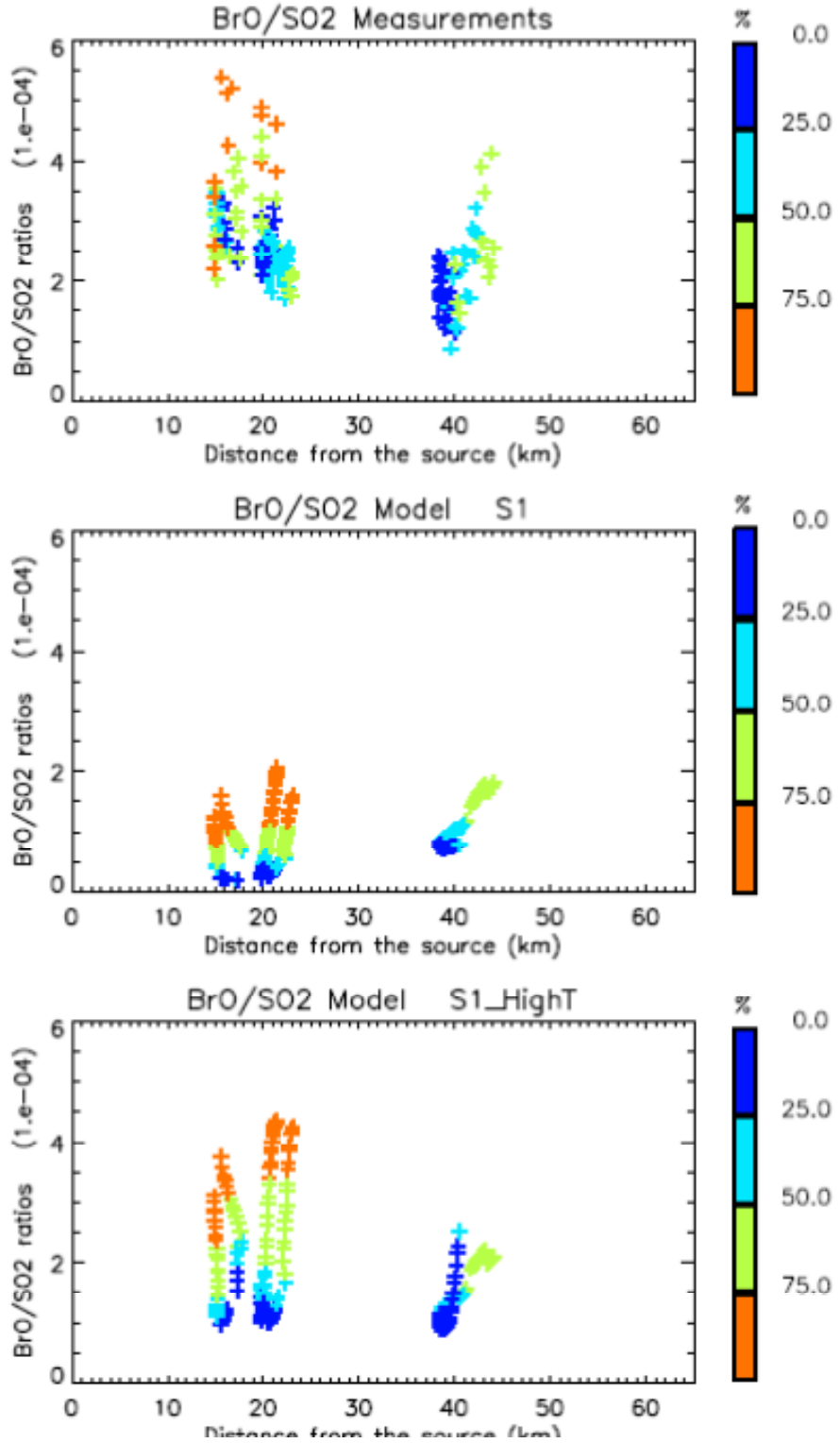

Figure 5: Variation of BrO/SO_2 ratios with distance from the vent derived from observations (top) and model simulations S1 (middle), S1_HighT (bottom) presented in Figure 3 and 4. For

each transect, each BrO/SO_2 ratio has been colored according to its SO_2 column value relative to the maximal value of the SO_2 column (SO2_max) for this transect. More precisely, the color indicates the relative difference $\frac{(SO2\_\max - SO2)}{SO2\_\max}$. Note that we did not include the observations nor the corresponding model results for which we did not have GPS data (dashed lines of Figures 3 and 4).

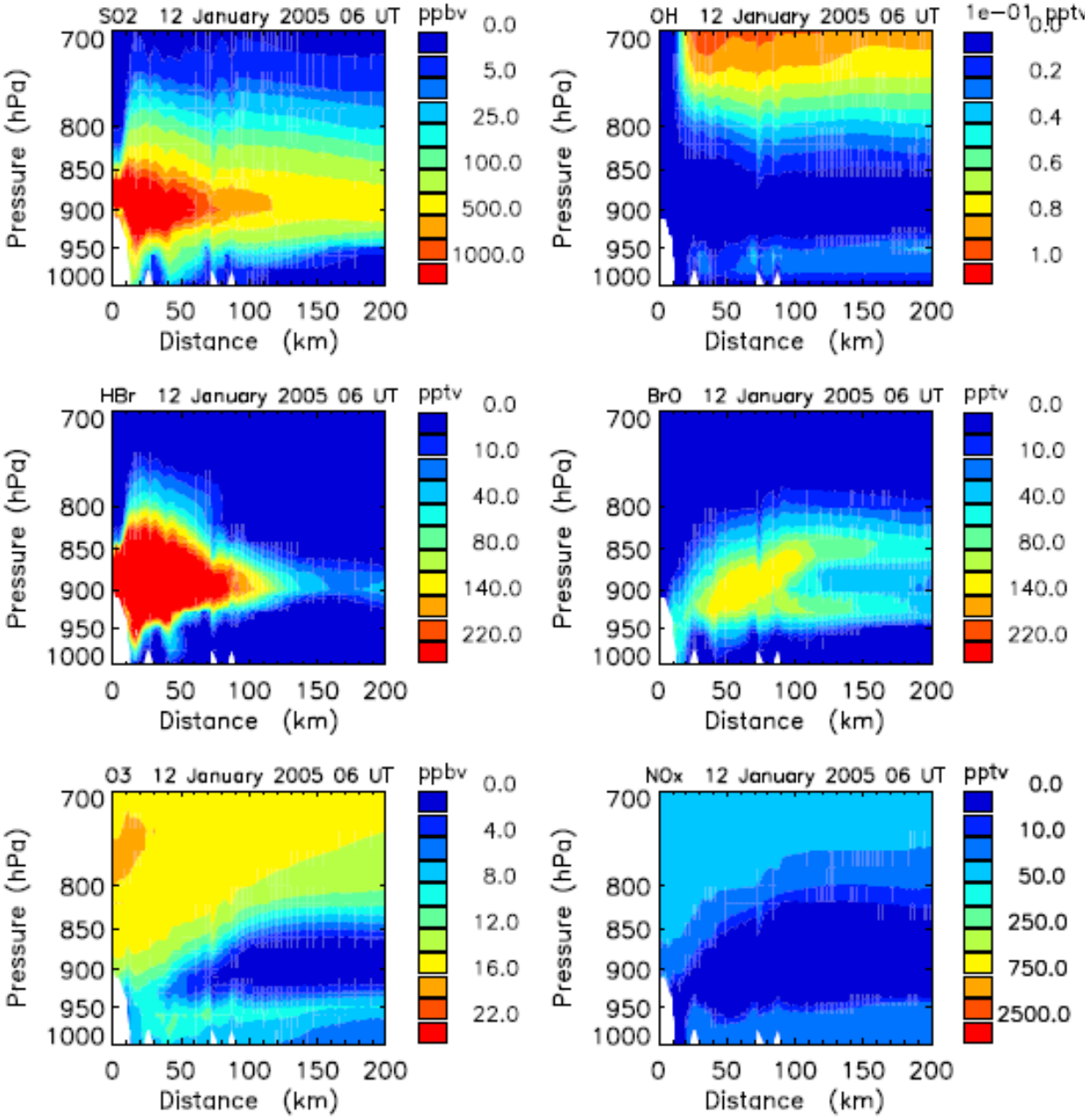

Figure 6: Distance-Pressure cross section of the SO_2, OH, HBr, BrO, O_3 and NO_x mixing ratios in the plume of Ambrym on 12th January 2005 at 06 UT in the simulation S1.

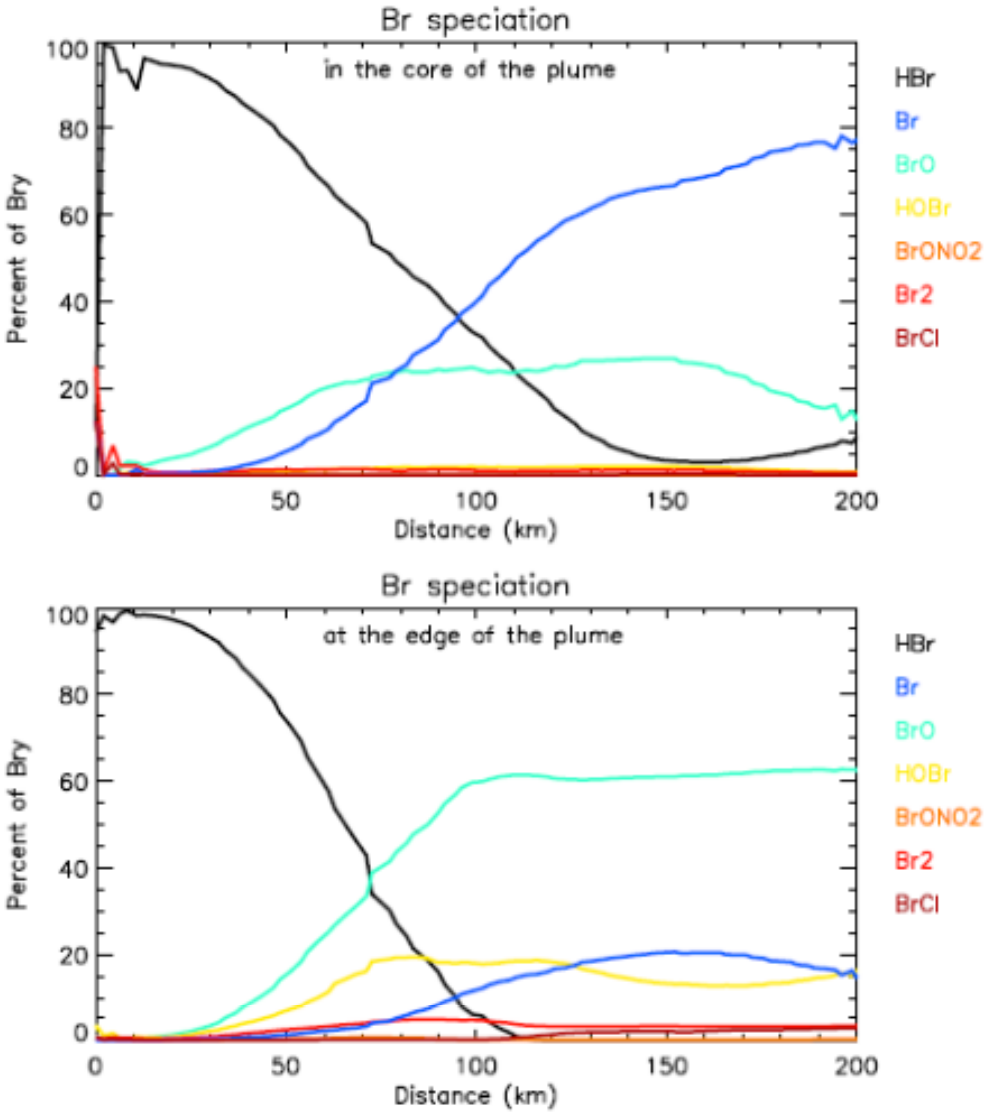

1697

1698

1699 **Figure 7**: Br speciation along the plume (in the core and at the edge) in the simulation S1 and

1700 the grid 2 km x 2 km the 12th of January 2005 at 06 UT. The Br speciation has been calculated

1701 as the percent of Bry (Bry= HBr + 2Br_2 + BrCl+ Br + BrO + HOBr + $BrONO_2$). Distance is

1702 calculated from the middle of the gridbox containing Marum and Benbow.

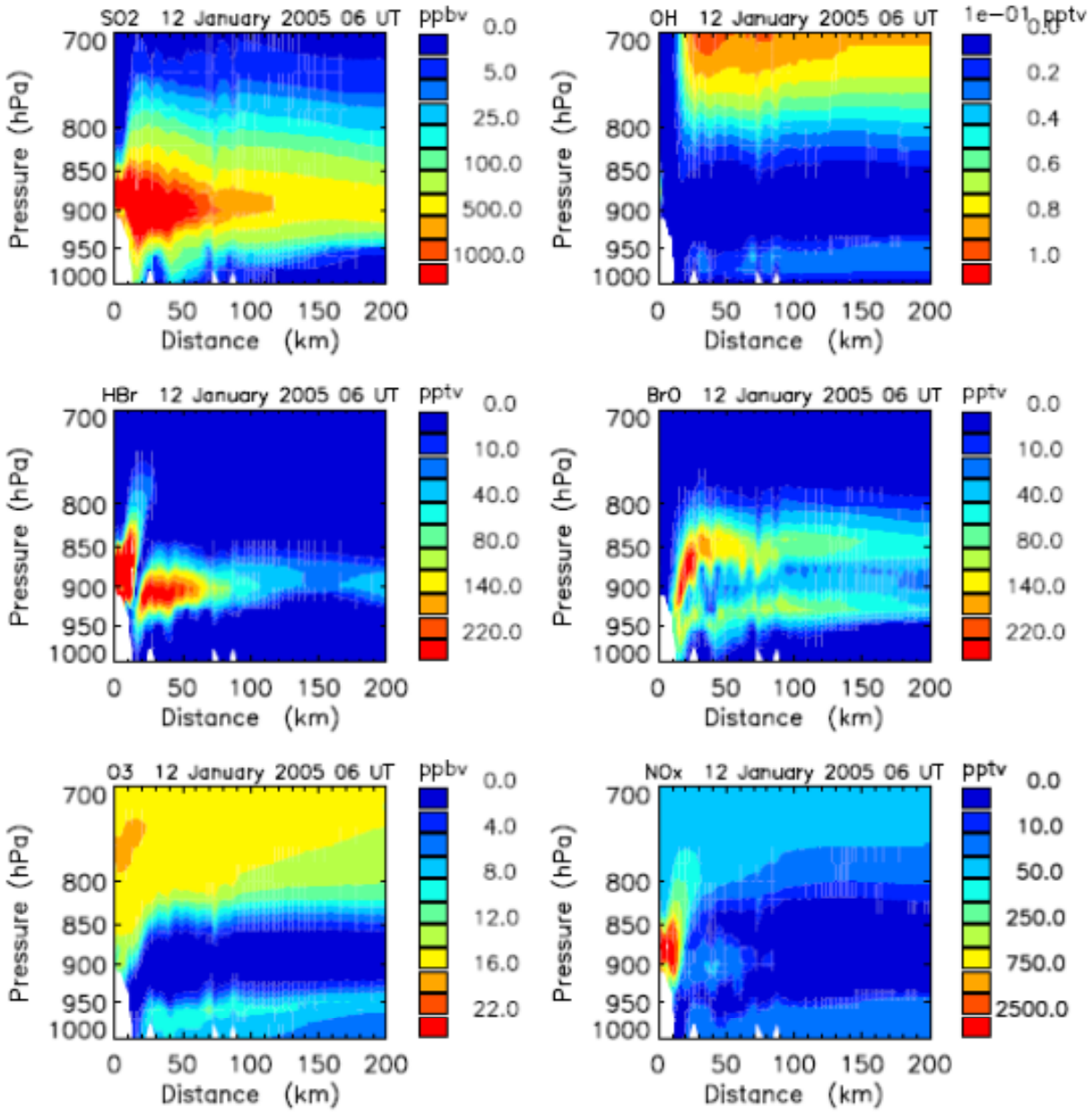

1703

1704

1705 **Figure 8:** Distance-Pressure cross section of the SO_2, OH, HBr, BrO, O_3 and NO_x mixing

1706 ratios in the plume of Ambrym on 12th January 2005 at 06 UT in the simulation S1_HighT.

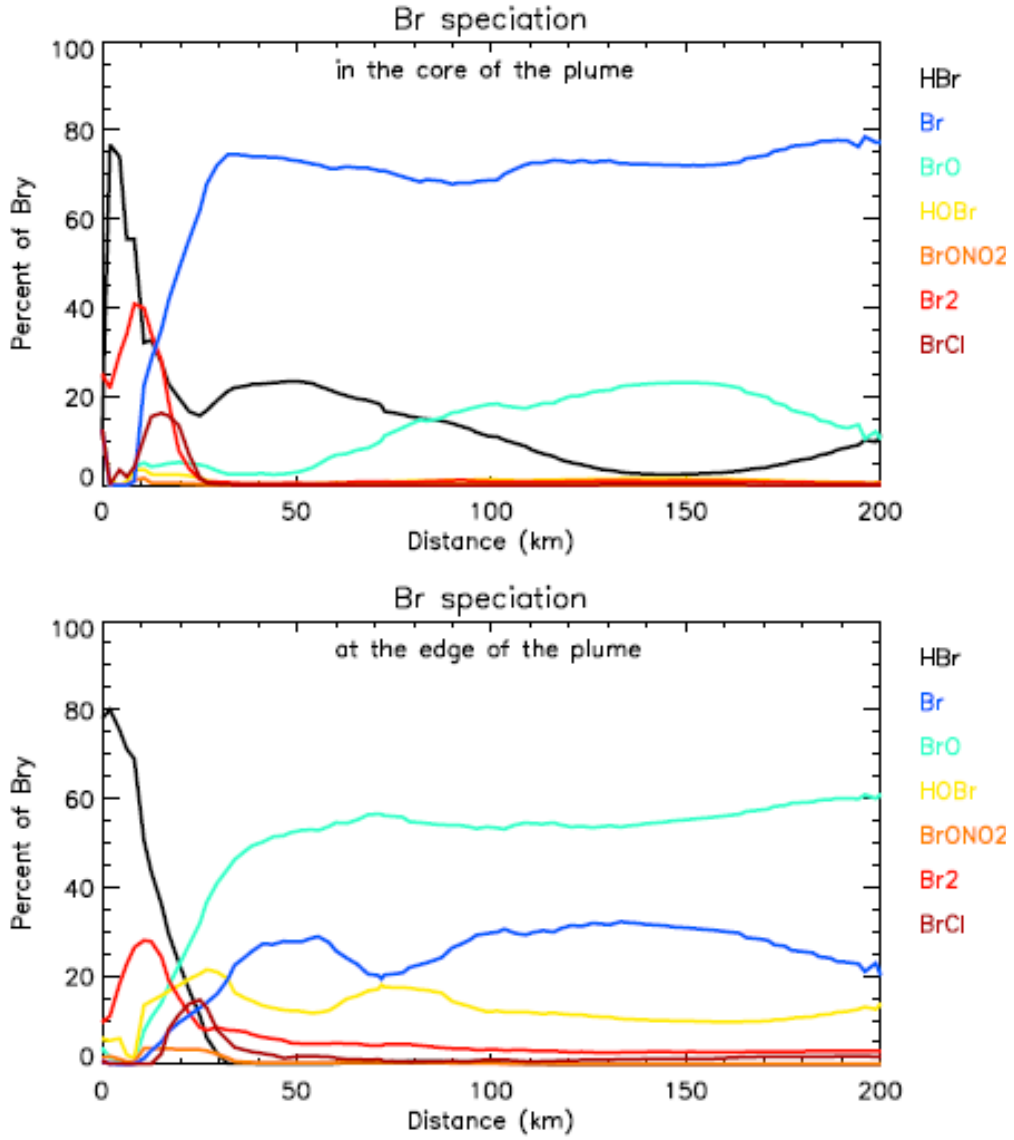

1707

1708

1709 **Figure 9:** Br speciation along the plume (in the core and at the edge) in the simulation
1710 S1_HighT and the grid 2 km x 2 km the 12th of January 2005 at 06 UT. The Br speciation has
1711 been calculated as the percent of Bry (Bry= HBr + $2Br_2$ + BrCl+ Br + BrO + HOBr +
1712 $BrONO_2$). Distance is calculated from the middle of the gridbox containing Marum and
1713 Benbow.

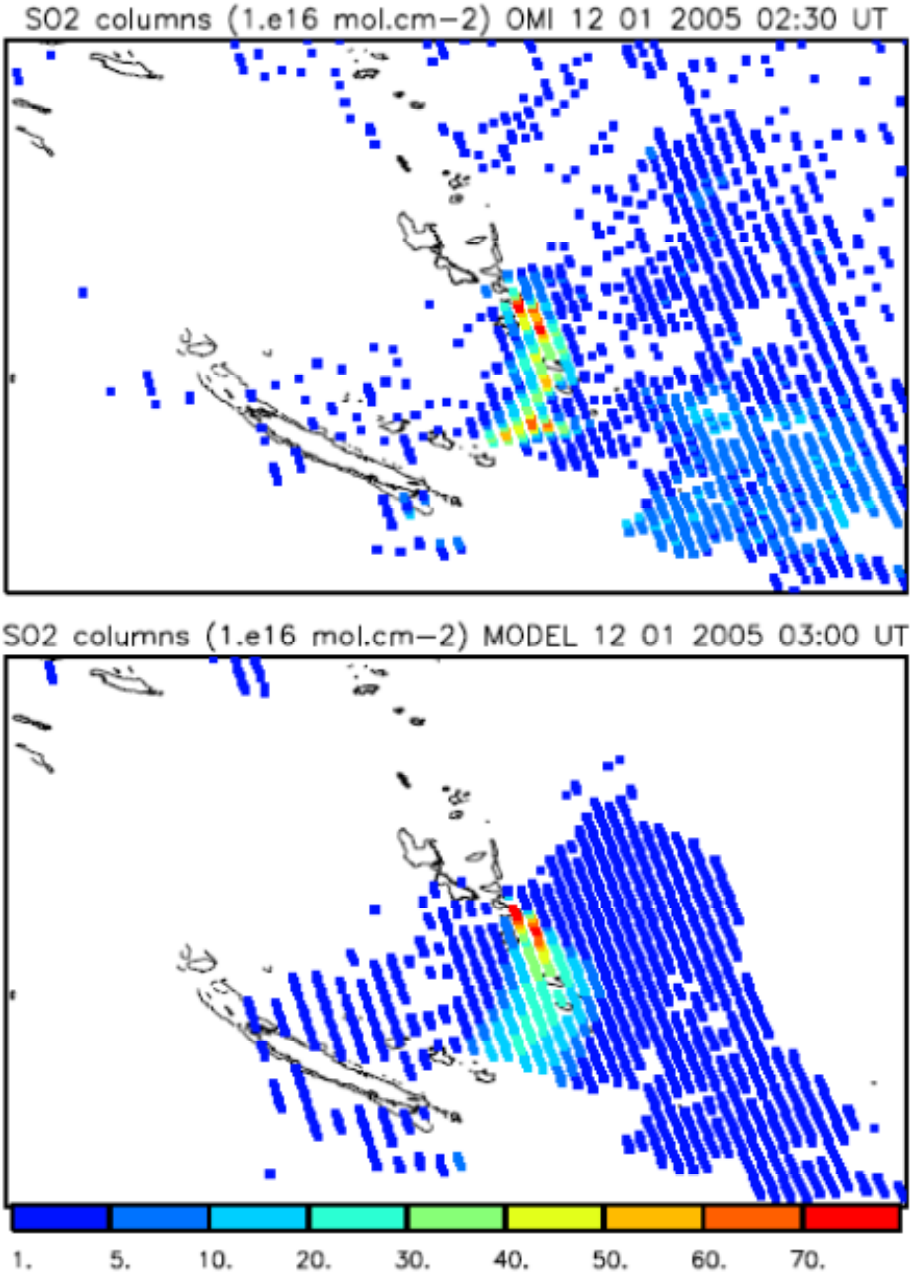

1714

1715

1716 **Figure 10**: Top: OMI SO_2 columns ($1x10^{16}$ molecule/cm^2) for the 12th January 2005 at 02 :

1717 30 UT. Bottom: Simulated SO_2 columns ($1x10^{16}$ molecule/cm^2) (S1_HighT) from the grid

1718 10km x 10km for the 12th January 2005 at 03:00 UT interpolated onto the OMI grid.

1719

1720

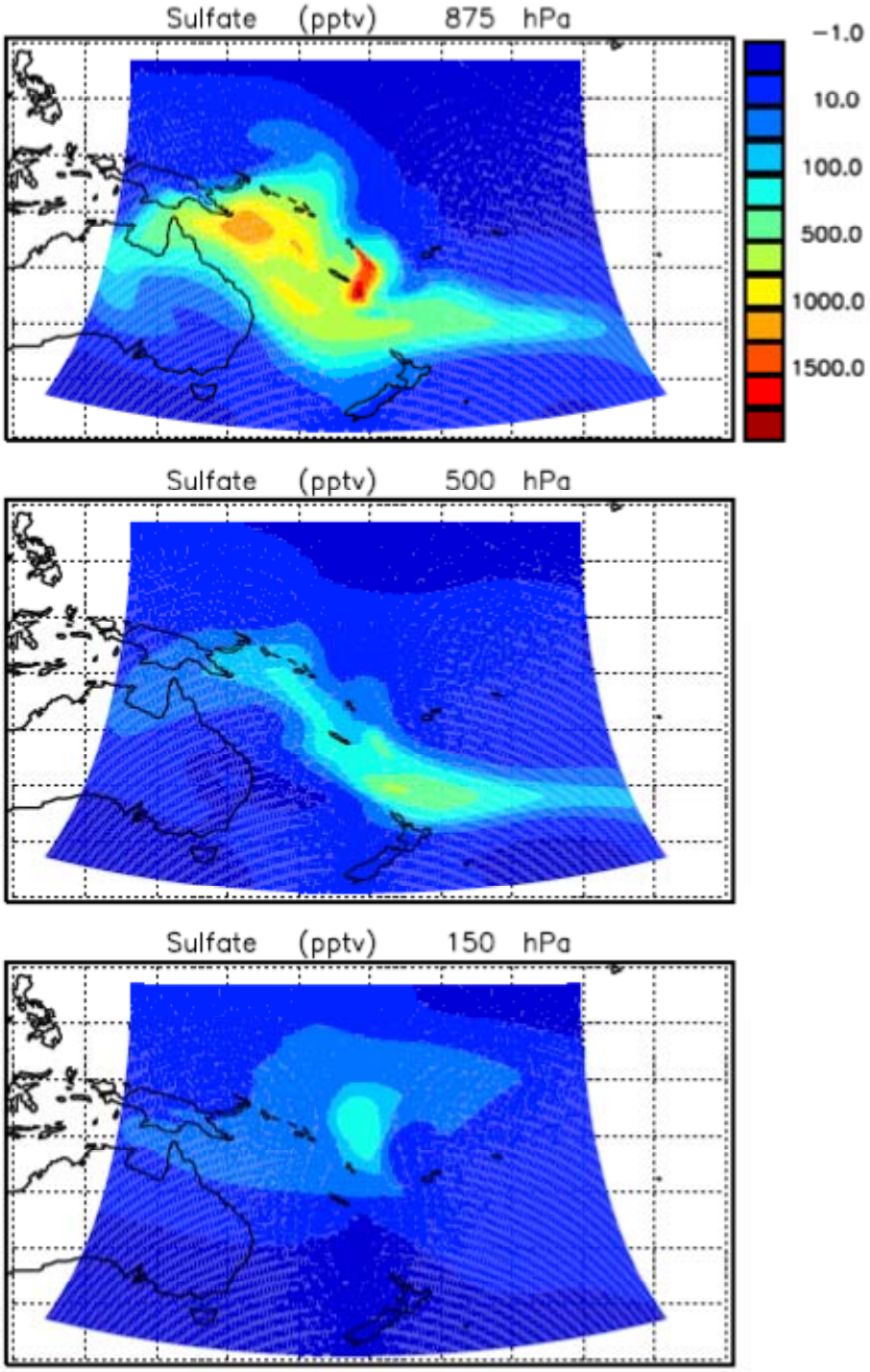

Figure 11: Daily mean difference (12th January 2005) between simulated sulfate in S1_HighT and in S0 at 875 hPa, 500 hPa and 150 hPa for the grid 50 km x 50 km.

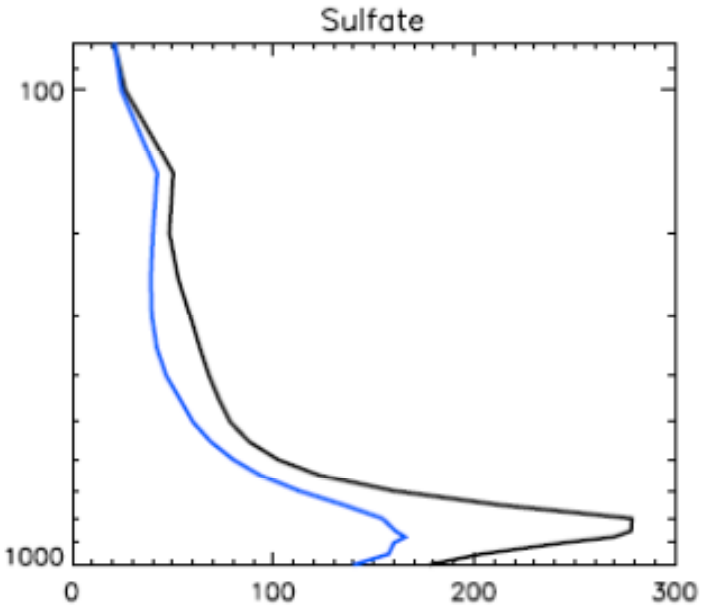

Figure 12: Profile of the daily (12th January 2005) mean mixing ratios (pptv) of sulfate simulated by the model in the larger grid (of resolution 50 km x 50 km) in S1_HighT (black) and in S0 (light blue).

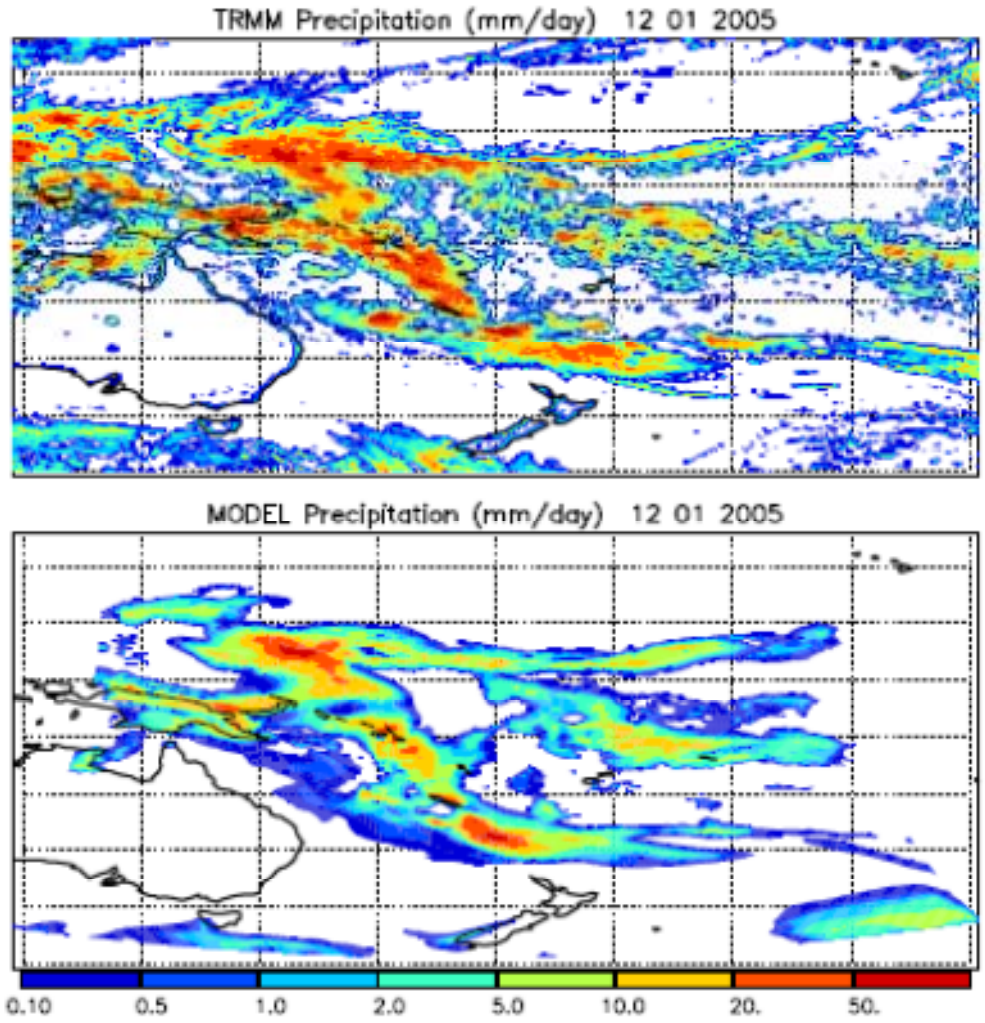

1735

1736

1737

1738 **Figure 13**: Daily precipitation (mm/day) for the 12th January 2005 as estimated from the

1739 TRMM satellite (3B42 product) and simulated by the model.

1740

1741

1742

1743

1744

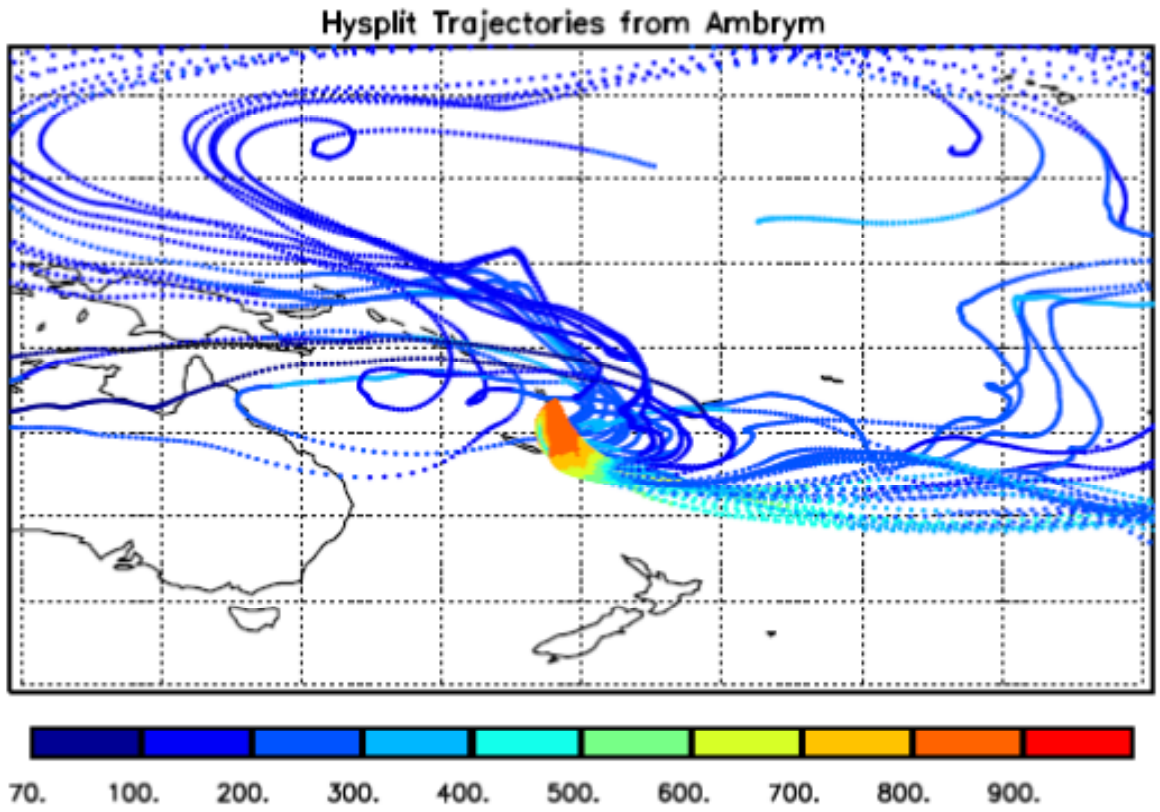

Figure 14: Fifteen-days forward trajectories initialized from the location of Ambrym volcano at 1373 m every hour on the 10th and 11th January 2005 calculated with the HYSPLIT model. The color scale represents the pressure (in hPa) of the air masses along the trajectories.

1758

1759

1760

1761

1762

1763

1764

1765

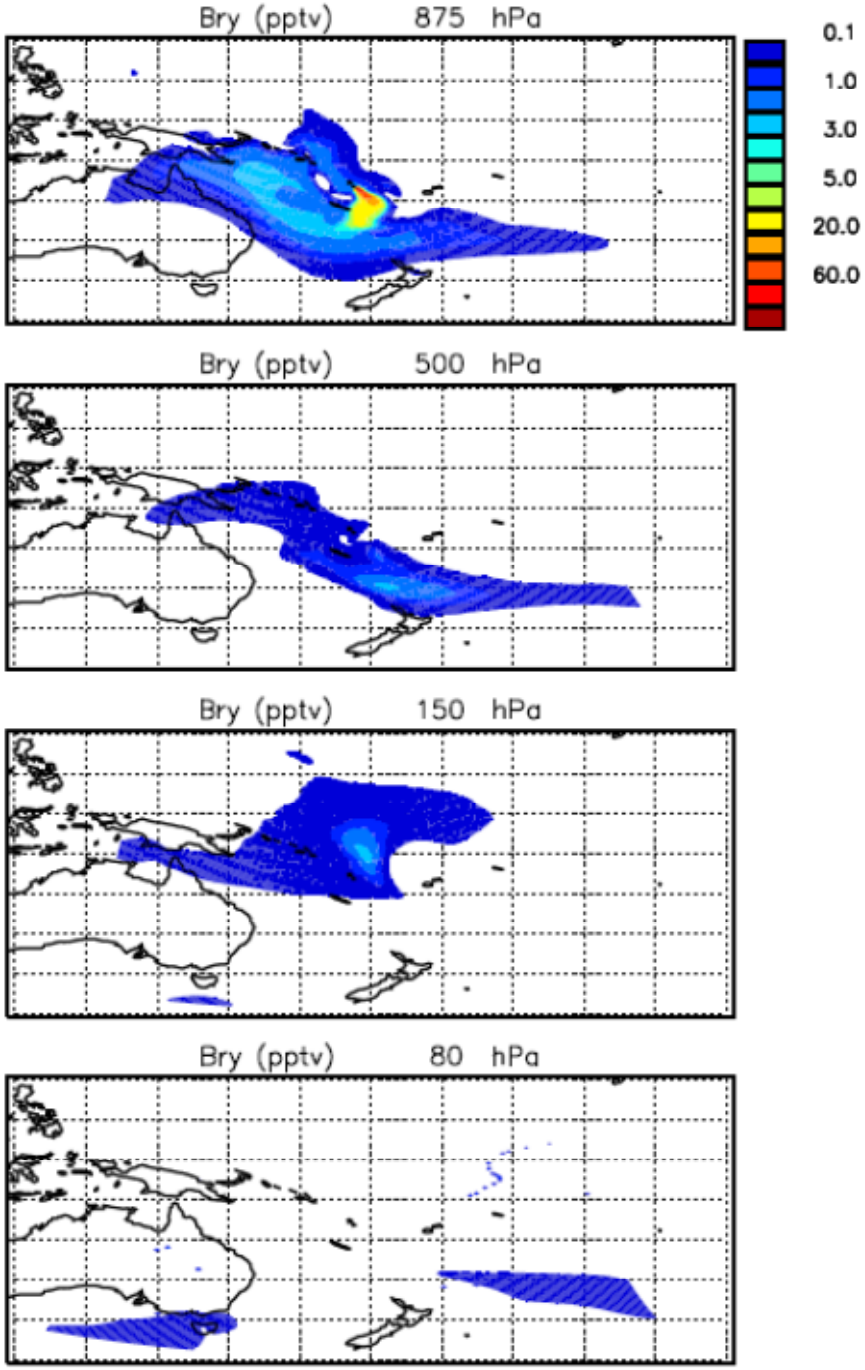

1766

1767

1768

1769 **Figure 15:** Daily mean difference (12th January 2005) between simulated Bry (pptv) in

1770 S1_HighT and in S0 at 875 hPa, 500 hPa, 150 hPa and 80 hPa for the 50 km x 50 km grid.

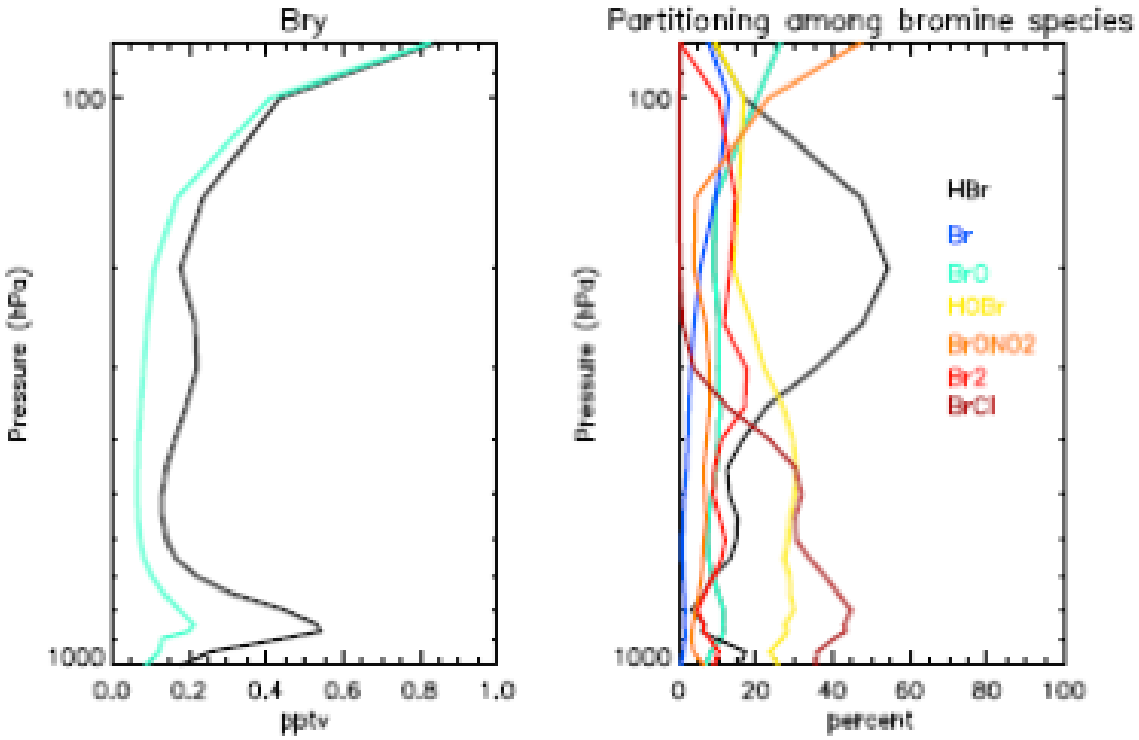

1771

1772

1773

1774

1775 **Figure 16:** Left: Profile of the daily (12th January 2005) mean mixing ratios of Br_y simulated

1776 by the model in the larger grid (50 km x 50 km) in S1_HighT (black) and in S0 (light blue).

1777 Right: Daily mean (12th January 2005) of the Br speciation (%) for the simulation S1_HighT

1778 for grid boxes where Bry mean difference between S1_HighT and S0 is larger than 0.5 pptv

1779 (Figure 15).

1780

1781

1782

1783

1784

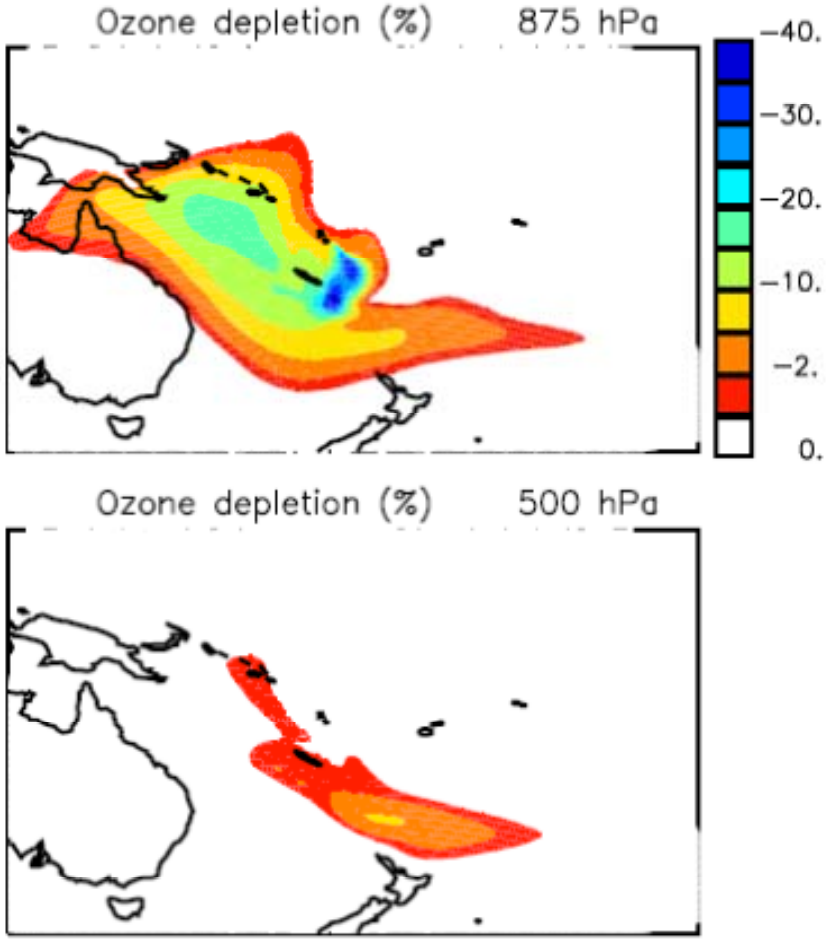

Figure 17: Daily mean difference (12th January 2005) between simulated ozone in S1_HighT and in S0 (in % relative to S0) at 875 hPa, 500 hPa for the 50 km x 50 km grid.